Estuarine Circulation, Mixing, and Residence Times in the Salish Sea

Parker MacCready[1,1], Ryan M. McCabe[1,1], Samantha A. Siedlecki[2,2], Marvin Lorenz[3,3], Sarah Nicole Giddings[4,4], Julia Bos[5,5], Skip Albertson[5,5], Neil Banas[6,6], and Soizic Garnier[6,6]

[1]University of Washington
[2]University of Connecticut
[3]Leibniz Institute for Baltic Sea Research
[4]University of California, San Diego
[5]Washington State Dept. of Ecology
[6]University of Strathclyde

November 30, 2022

Abstract

A realistic numerical model is used to study the circulation and mixing of the Salish Sea, a large, complex estuarine system on the United States and Canadian west coast. The Salish Sea is highly productive and supports many important fisheries but is threatened by recurrent hypoxia and ocean acidification, so a clear understanding of its circulation patterns and residence times is of value. The estuarine exchange flow is quantified at 39 sections over three years (2017-2019) using the Total Exchange Flow method. Vertical mixing in the 37 segments between sections is quantified as opposing vertical transports: the efflux and reflux. Efflux refers the rate at which deep, landward-flowing water is mixed up to become part of the shallow, seaward-flowing layer. Similarly, reflux refers to the rate at which upper layer water is mixed down to form part of the landward inflow. These horizontal and vertical transports are used to create a box model to explore residence times in a number of different sub-volumes, seasons, and years. Residence times from the box model are generally found to be longer than those based on simpler calculations of flushing time. The longer residence times are partly due to reflux, and partly due to incomplete tracer homogenization in sub-volumes. The methods presented here are broadly applicable to other estuaries.

1

2 **Estuarine Circulation, Mixing, and Residence Times in the Salish Sea**

3 **P. MacCready[1], R. M. McCabe[2,3], S. A. Siedlecki[4], M. Lorenz[5], S. N. Giddings[6], J. Bos[7], S.**

4 **Albertson[7], N. S. Banas[8], S. Garnier[8]**

5 [1]University of Washington, School of Oceanography.

6 [2]University of Washington, Joint Institute for the Study of the Atmosphere and Ocean, Seattle,

7 WA, USA.

8 [3]University of Washington, Cooperative Institute for Climate, Ocean, and Ecosystem Studies,

9 Seattle, WA, USA.

10 [4]University Connecticut, Department of Marine Sciences.

11 [5]Leibniz Institute for Baltic Sea Research Warnemünde, Rostock, Germany.

12 [6]University of California, San Diego.

13 [7]Washington State Department of Ecology.

14 [8]University of Strathclyde.

15 Corresponding author: Parker MacCready (pmacc@uw.edu)

16 **Key Points:**

17 • The estuarine circulation throughout the Salish Sea is estimated over three years from a
18 realistic numerical model, focusing on the exchange flow.

19 • The vertical mixing, or "reflux" is stronger at sills, but is also large when integrated over
20 the basins between sills.

21 • Residence time is calculated in three ways, quantifying the extent to which it is increased
22 (often more than doubled) by reflux and incomplete homogenization within a volume.

23

24 **Abstract**

25 A realistic numerical model is used to study the circulation and mixing of the Salish Sea, a large,

26 complex estuarine system on the United States and Canadian west coast. The Salish Sea is

27 biologically productive and supports many important fisheries but is threatened by recurrent

28 hypoxia and ocean acidification, so a clear understanding of its circulation patterns and residence

29 times is of value. The estuarine exchange flow is quantified at 39 sections over three years

30 (2017-2019) using the Total Exchange Flow method. Vertical mixing in the 37 segments

31 between sections is quantified as opposing vertical transports: the efflux and reflux. Efflux

32 refers the rate at which deep, landward-flowing water is mixed up to become part of the shallow,

33 seaward-flowing layer. Similarly, reflux refers to the rate at which upper layer water is mixed

34 down to form part of the landward inflow. These horizontal and vertical transports are used to

35 create a box model to explore residence times in a number of different sub-volumes, seasons, and

36 years. Residence times from the box model are generally found to be longer than those based on

37 simpler calculations of flushing time. The longer residence times are partly due to reflux, and

38 partly due to incomplete tracer homogenization in sub-volumes. The methods presented here are

39 broadly applicable to other estuaries.

40 **Plain Language Summary**

41 The Salish Sea is a large estuarine system that includes the cities of Vancouver on the Strait of

42 Georgia and Seattle on Puget Sound. Despite the many rivers flowing into the Salish Sea, the

43 water in the system is mostly ocean water, and there is rapid exchange with the ocean. This

44 exchange is important because it brings in most of the nutrients that feed the ecosystem, and it

45 flushes the system relatively rapidly, leading to generally good water quality. Nonetheless, there

46 are places and times in the Salish Sea that experience problems like hypoxia and fish kills. The

47 goal of this work is to clearly describe the patterns of circulation and mixing throughout the

48 Salish Sea so that we may understand the causes and potential future changes in these water

49 quality problems. We use a realistic computer simulation, tested against many observations, to

50 predict the circulation and mixing patterns. We then use those currents to estimate residence

51 times in different parts of the Salish Sea for different seasons and years. The most important

52 result is that we find that the mixing of surface water with deep water can distribute water

53 properties throughout the Salish Sea, increasing the residence time.

1 Introduction

The exchange flow is widely recognized as a defining property of tidally averaged estuarine circulation. The persistent inflow of deep, salty water and outflow of shallow, somewhat fresher water is often many times greater in volume flux than all the rivers entering a system. As a result, the exchange flow controls residence times and biogeochemical gradients. Physically this circulation is a result of the density contrast between ocean and river water, combined with mixing and advection from tidal currents (Geyer & MacCready, 2014; MacCready & Geyer, 2010). The theory of estuarine exchange flow was developed and tested for shallow, straight coastal plain estuaries such as the Hudson (Hansen & Rattray, 1965; Ralston et al., 2008) but is less well-developed for more complex systems. In this paper we focus on the circulation of one of these complex systems - the Salish Sea, a large, interconnected system of very deep basins and shallow straits forced by strong tides and many rivers. Despite the extreme bathymetric irregularity of the Salish Sea, it develops a vigorous exchange flow (Bretschneider et al., 1985; Geyer & Cannon, 1982; D. A. Sutherland et al., 2011; Richard E. Thomson et al., 2007). The deep inflow and shallow outflow through the mouth of the system average around 140,000 m^3 s^{-1}, about 70% of the flow of the Amazon River. This is one of the largest exchange flows on the planet, although it is only about 1/7th the magnitude of the inverse estuarine circulation of the Mediterranean Sea (Pinardi et al., 2019).

A key insight of early researchers was that the Salish Sea may be thought of as a system of large, relatively quiescent basins, joined by straits with strong tidal currents and mixing (Ebbesmeyer & Barnes, 1980). The mixing at straits causes "reflux" in which a significant amount, perhaps up to half (Ebbesmeyer et al., 1988) of the outflowing branch of the exchange flow is mixed down and becomes part of the inflowing branch of the exchange flow. The implications for residence time were recognized immediately: refluxing could mean that it takes much longer for the system to flush out conservative tracers. The mathematical framework for reflux was developed rigorously by Cokelet and Stewart (1985) calling it "efflux/reflux" (efflux is the water mixed up which then heads seaward; reflux is the water mixed down which then heads landward). In the present work we use three years of a realistic numerical simulation and new analytical tools to calculate the size and consequences of exchange and reflux in the Salish Sea.

83 A history of circulation studies in the region is given in Section 2. The model setup and

84 evaluation against data are presented in Section 3, with more detail given in the Supplementary

85 text. The analysis of model fields to calculate the exchange flow and efflux/reflux throughout

86 the system is given in Section 4. A box model is constructed using these transports. Box model

87 results focusing on the residence time are given in Section 5. Further discussion is provided in

88 Section 6.

89 We find that the exchange flow varies smoothly along the system, increasing nearly linearly

90 from the landward bays to the seaward end at the Strait of Juan de Fuca (Fig. 1), consistent with

91 findings in D. A. Sutherland et al. (2011). This finding is not consistent with the exchange flow

92 being interrupted at the sills as hypothesized in Ebbesmeyer and Barnes (1980). This smooth

93 variation we find is often seen in coastal plain estuaries, but is perhaps not expected in a place

94 like the Salish Sea where mixing is tightly concentrated at a few energetic sills (Ebbesmeyer et

95 al., 1988; Gregg & Pratt, 2010; Seim & Gregg, 1994). Use of the Total Exchange Flow method

96 (MacCready, 2011) is required for correct estimation of the exchange flow in places where the

97 salt flux is significantly influenced by tidal correlation of salinity and transport. We also find

98 that the vertical efflux/reflux transports, while strongest at sills, are also important throughout the

99 basins when considered as an area integral. The box model is used to calculate the movement of

100 passive tracers in the Salish Sea in different years and seasons. From it we find that residence

101 times which account for reflux, and for incomplete homogenization within basins, may be two or

102 more times longer than standard flushing times.

103 **2 A brief history of studies of Salish Sea Circulation**

104 The pattern and variability of circulation, mixing, and water properties in the Salish Sea has been

105 the subject of many studies in the past seven decades. The overall conclusion is that the system

106 functions like an estuary, with strong, localized mixing and a very large exchange flow despite

107 the fjord-like, glacier-carved basins. Early data on water properties in Puget Sound was

108 collected in 1952-1966 and presented in hand-contoured plots in Collias et al. (1974). Similarly,

109 Crean and Ages (1971) present observations from twelve cruises in 1968 in the Straits of

110 Georgia and Juan de Fuca (see Fig. 1 for place names). Early studies of Juan de Fuca prompted

111 its inclusion as an extreme end member in the famous Hansen and Rattray (1965) paper on the

112 physics of the estuarine exchange flow.

113   Spurred by concerns over the fate of contaminants in the system and the causes of hypoxia,

114   observational studies accelerated greatly in the 1970's. Early Canadian research is reviewed in

115   LeBlond (1983), highlighting important current meter observations of the average exchange flow

116   in Juan de Fuca and Johnstone Strait (the channel at the northern end of Strait of Georgia that

117   connects to the Pacific). On the U.S. side of the international border the National Oceanic and

118   Atmospheric Administration (NOAA) initiated the MESA (Marine Ecosystems Analysis) Puget

119   Sound Program, with results reviewed in Ebbesmeyer et al. (1988) and many NOAA reports.

120   Simultaneously, large advances were made in understanding the complex pattern of tides

121   (Lavelle et al., 1988; Mofjeld & Larsen, 1984) that are the dominant factor governing currents

122   and mixing in the Salish Sea. While Puget Sound has been the subject of a great deal of study, it

123   only comprises about 8% of the nearly 2000 km^3 volume of the Salish Sea.

124   In the four decades since 1980 there have been many observational studies of the Salish Sea

125   ecosystem and circulation. Notable additions to our knowledge have come from the

126   accumulation of long time series from sustained observational programs such as the extensive

127   seasonal surveys conducted by the Canadian Institute of Ocean Sciences (Masson & Peña, 2009),

128   and the Washington (WA) State Dept. of Ecology monthly CTD stations initiated around 1990.

129   Long term change and interannual variability are summarized in Riche et al. (2014) where the

130   gradual warming of the system, and other changes, are made apparent.

131   Evolving with, and somewhat lagging behind the observational advances, modeling has emerged

132   as a useful scientific tool for Salish Sea studies. The fact that accurate 3-D models of the system

133   only arrived in the last decade is due to the extreme bathymetric complexity of the Salish Sea.

134   This complexity prompted the early creation of simpler models that could be used to predict

135   high-value quantities such as residence time. These typically divide the region into a number of

136   segments horizontally and two layers vertically. Cokelet et al. (1991) developed such a model for

137   Puget Sound, exploiting the Knudsen (1900) relations to diagnose the exchange flow from

138   known river flow and salinity distributions; see Burchard et al. (2018) for a translation of

139   Knudsen's paper. A similar approach, allowing for time-dependence, is presented in Hagy et al.

140   (2000) for a tributary of the Chesapeake. Li et al. (1999) used a more dynamical approach in a

141   box model of the Strait of Georgia – Juan de Fuca system, incorporating a physical

142   parameterization of exchange as a function of along channel density gradients. Babson et al.

143   (2006) used a similar dynamical approach in a box model of Puget Sound. A novel two-tracer

144 approach to diagnosing the exchange flow and mixing, applied to parts of the Salish Sea, is

145 presented in R. Pawlowicz (2001).

146 Realistic models of the Salish Sea were also attempted in past decades but were significantly

147 hampered by lack of computing power. Modern, realistic models of the Salish Sea only

148 appeared in the last decade (Khangaonkar et al., 2017; Khangaonkar et al., 2011; Moore et al.,

149 2015; Olson et al., 2020; Peña et al., 2016; Soontiens et al., 2015; D. A. Sutherland et al., 2011).

150 The present model continues this realistic numerical approach.

151 **3 Model Setup and Evaluation**

152 The realistic numerical model used here is created using the Regional Ocean Modeling System

153 (ROMS) (Haidvogel et al., 2000; Shchepetkin & McWilliams, 2005) which integrates the

154 Reynolds averaged, Boussinesq, incompressible equations of motion and tracer concentration on

155 a rotating, spherical grid. The model configuration used here is called LiveOcean. The model

156 domain covers all of Oregon, Washington, and Vancouver Island coastal waters, and the Salish

157 Sea – the name for the combined inland waters of Puget Sound, Strait of Georgia, and the Strait

158 of Juan de Fuca (Fig. 1). The model grid follows lines of constant longitude and latitude, with

159 500 m spacing in most of the Salish Sea and Washington coastal estuaries, stretching up to 3 km

160 at open boundaries. There are 30 vertical levels, following the bathymetry and free surface. The

161 model is configured to be as realistic as possible, with 45 rivers, 8 tidal constituents, open ocean

162 conditions from a global data-assimilative model, and high-resolution atmospheric forcing from

163 a regional weather forecast model. The model builds upon prior realistic configurations focused

164 inside of the Salish Sea (D. A. Sutherland et al., 2011) and on the open coast (Giddings et al.,

165 2014). Details of the model setup are given in Supplementary Text S1. The model run analyzed

166 here was initialized December 15, 2016 and runs through the present because it makes quasi-

167 operational daily forecasts. Here we work only with the three-year period 2017-2019. During

168 2019 the Salish Sea experienced low river flows (Fig. 1c) causing the system to grow

169 progressively saltier.

170 The three-year model hindcast has been extensively compared to observations. A summary of

171 those comparisons is presented in Supplementary Text S2. Focusing on one aspect of the

172 evaluation most relevant to the exchange flow, along-channel sections of the salinity for 2017 are

173   plotted in Fig. 2. Here we use the cast data averaged over the upper and lower parts of the water

174   column at CTD stations to test the model skill at reproducing the along-channel salinity gradient

175   and stratification. The along-channel salinity gradient is thought to provide the driving pressure

176   gradient for the estuarine exchange flow (Giddings & MacCready, 2017; MacCready & Geyer,

177   2010) and the size of the exchange flow as estimated from Knudsen's Relations depends

178   critically on the stratification. Evaluating these for the three Puget Sound along-channel sections

179   shown in Fig. 2 we find that the model salinity gradient is somewhat too weak, being 78-85% of

180   that observed. The model stratification is 64-116% of that observed, with the lower value

181   representative of model performance in Hood Canal. The stratification results are most easily

182   related to the exchange flow because the Knudsen's Relations state that the exchange flow is

183   inversely proportional to the stratification (Burchard et al., 2018), so this range suggests our

184   exchange transports may be overestimated by as much as 56% or underestimated by as much as

185   14%. As mentioned in Supplementary Text S2, there was a significant temporal increase of

186   salinity in the Salish Sea: 0.68 g kg^{-1} over three years estimated from CTD data. Comparing to

187   these data, the salinity bias of the model for stations inside Puget Sound stayed roughly the same

188   in each year (0.62, 0.60, 0.53) implying that the modeled salinity drift was capturing a real trend,

189   and not a spurious model artifact.

190   **4 Calculation of the Exchange Flow and Mixing**

191   The analysis of modeled circulation in the Salish Sea is done in three steps. Our focus will be on

192   subtidal and longer timescales, and on how the exchange flow and mixing affect residence times

193   and tracer concentrations in general. In the first step we calculate the tidally averaged exchange

194   flow, following methods described in MacCready (2011), through many sections (Fig. 3).

195   Second, we make seasonal and annual averages of the two-layer exchange flow and use these to

196   calculate vertical mixing rates throughout the system. Finally, we use the overall pattern of

197   horizontal transports (the exchange flow) and vertical transports (mixing) to construct an

198   efficient box model of the Salish Sea. The box model is used to explore residence times in

199   different years and seasons. The box model is also used to calculate the concentration and age of

200   a tracer injected from various sources such as a river.

201   4.1 The Total Exchange Flow

202   The exchange flow is calculated at 39 cross-sections throughout the Salish Sea (Fig. 3). At each

203   section we extract hourly snapshots of section-normal transport and salinity in each grid cell.

204   The sections are aligned with the model grid and located on velocity points of the ROMS C-grid,

205   e.g. for a N-S section such as *jdf1* the cross section is on the model u-grid. Keeping the sections

206   on the model grid minimizes interpolation errors (MacCready, 2011). The three-year average

207   error in the system-wide volume budget is 0.42% of the average net river flow, and the error in

208   the salt budget is 0.016% of the average salt flux of the inward exchange flow. The largest error

209   found was 2.44% for the Hood Canal 2018 volume budget. For any budget calculations it is

210   essential that volume be conserved as well as possible since any errors in volume transport will

211   propagate through all tracer transport calculations. Comparing the error to mean river flow in a

212   basin, as we do here, is a conservative approach because typically the exchange flow transports

213   are an order of magnitude larger.

214   The exchange flow is calculated at each section using the Total Exchange Flow (TEF) method

215   (MacCready, 2011). Here transport is sorted into salinity classes, tidally averaged and then the

216   sum of the transport in all inward flowing salinity classes is called Q_{in}. The flux-weighted

217   salinity of the inflow is S_{in}. Similarly, the outflow is quantified as Q_{out} and S_{out}. The sign

218   convention is that Q_{out} is negative. These TEF variables thus consist of four tidally averaged

219   time series at each section. The reason for using salinity classes is that it accounts for tidal

220   variation in the spatial structure of the salt flux (MacCready, 2011). The TEF variables give the

221   total inward and outward salt flux through a section as $Q_{in}S_{in} + Q_{out}S_{out}$ regardless of whether the

222   salt flux was due to steady exchange flow or tidal pumping. TEF has been found to give a clear

223   representation of the exchange flow in many systems (Burchard et al., 2018; Chen et al., 2012;

224   Conroy et al., 2020; Geyer & MacCready, 2014; Lorenz et al., 2020; Rayson et al., 2017; D. A.

225   Sutherland et al., 2011). Using the TEF method is especially appropriate in the Salish Sea

226   because the system is known to have large basins with exchange organized by depth (deep saltier

227   inflow, shallow fresher outflow) punctuated by energetic sill like Tacoma Narrows where the

228   exchange is organized by time (saltier flood, fresher ebb).

229   We calculate transport in 1000 salinity bins and then integrate over these to form inflowing and

230   outflowing layers using the "dividing salinity" method (MacCready et al., 2018) which has been

231   shown to give reliable results even for nearly well-mixed cases (Lorenz et al., 2019). We allow

232   for the existence of more than two layers in calculating our initial layer averages (Lorenz et al.,

233   2019), but then combine these into just two layers, conserving net salt flux in either direction.

234   An example of the results is plotted as time series for section *ai3* in Fig. 4. At this section there

235   is a clear annual cycle of the salinity of the two layers, growing saltier and with less salinity

236   difference between in- and outflow in the late fall when river flows have been low for some

237   months. The daily values show evidence of increased salinity of the inflow during weak neap

238   tides (Fig. 4a), consistent with the observations of Geyer and Cannon (1982). The exchange

239   flow transport (Fig. 4b) also shows annual and fortnightly variation. The dynamics controlling

240   these is of great importance but will not be addressed in this paper because we are focusing

241   instead on describing the circulation and its implications for residence time. About half of the

242   sections could be characterized as having more than two layers at times, and this is an important

243   caveat on our subsequent calculations using transports that have been expressed somewhat

244   artificially as two layers. A more nuanced approach allowing three or four layers is presented in

245   Rich Pawlowicz et al. (2007) for the Strait of Georgia. We proceed by assuming that a two-layer

246   estuarine circulation is adequate for understanding the broad patterns of circulation in the Salish

247   Sea, but caution that the details of stratification and water residence time in a given basin are best

248   handled by calculations using a realistic model, albeit at substantially greater computing cost.

249   The two-layer transports for all sections averaged over 2017 are plotted in Fig. 5. In general, the

250   magnitude of the exchange flow transport increases steadily moving seaward. However, the

251   increase is not perfectly monotonic, e.g. between sections *tn2* and *tn3* at Tacoma Narrows (Fig.

252   5b). This is consistent with previous results (D. A. Sutherland et al., 2011) that also used the

253   TEF method. The results are inconsistent with the characterization of the Salish Sea circulation

254   presented in Ebbesmeyer and Barnes (1980) and Khangaonkar et al. (2017) which did not use the

255   TEF method. The places where our results differ most is at the sills, with the exchange flow in

256   Khangaonkar et al. (2017) at Admiralty Inlet being about half what we find, and that in Tacoma

257   Narrows being about one-tenth of what we find. This is not to say that the Khangaonkar et al.

258   (2017) model is incorrect; indeed it has circulation patterns and validation statistics that are

259   similar to what we present here. The difference is that the TEF method is required to correctly

260   quantify the exchange flow at energetic places like sills where salt flux due to tidal pumping may

261   be an important mechanism. This is because at sills there is local enhancement of tidal currents

262   and often distortions of the salinity field due to rough bathymetry that may lead to local tidal

263   correlation of salinity and transport (i.e. tidal pumping). The TEF method, by construction,

264   includes tidal pumping as part of the net advective flux. This distinction is important for our

265   understanding of the circulation of the Salish Sea. In Ebbesmeyer and Barnes (1980) the

266   circulation was described as a two layer flow that was interrupted at sills, with the seaward-

267   flowing surface layer being largely sent downward by refluxing at a sill, resulting in a conceptual

268   model in which the basins were much more isolated from each other than our calculations

269   suggest. Nonetheless, there is a lot of vertical mixing and refluxing of water at sills, but it does

270   not interrupt the horizontal exchange flow in the way envisioned by previous authors. We

271   explore this distinction further below. More TEF section results are given in the Supplementary

272   Text S3, showing patterns of tidal energy flux and net volume transport.

273   The TEF properties are a compact way to represent the system behavior. A three-year time

274   series of S_{in} and S_{out} for the Puget Sound sub-volume (with bounding sections at *ai1* and *dp*) is

275   plotted in Fig. 6a. Also plotted is the volume-mean salinity over that time period, which

276   increases by about 0.7 g kg^{-1} while the salinity difference between inflow and outflow, $\Delta S \equiv$

277    $S_{in} - S_{out}$, decreases. The exchange flow over that time did not exhibit a clear multi-year trend

278   (Fig. 6b), although it does have a strong annual cycle, peaking in winter when the river flow

279   (Fig. 6d) is strong. The annual mean river flows entering Puget Sound were close to average in

280   2017, dropped a bit in 2018, and dropped by a third in 2019 (Fig. 6d). Similar budgets (not

281   shown) were formed for other sub-volumes of the Salish Sea, and for the complete system, and

282   in all cases the salinities had a sensible relationship to the net river flow: during times of low

283   flow like the late summer or 2019 the salinity was increasing and ΔS was decreasing. The

284   exchange flow, in contrast, was much harder to explain. There was no consistent phasing

285   between exchange flow and net river flow, nor was there an interannual trend. This may

286   represent the unusual plumbing of the system. Taking the Puget Sound volume (Fig. 6) as an

287   example, the biggest freshwater source in the Salish Sea is seaward of Puget Sound and peaks

288   some months later than Puget Sound Rivers (Fig. 1). The exchange flow may also be influenced

289   by the density of water upwelled on the coast during spring and summer (Babson et al., 2006),

290   the seasonal variation of wind (D. A. Sutherland et al., 2011), and tides (Deppe et al., 2018).

291   A complete salt budget may be formed from the TEF quantities, and the terms may be expressed

292   most clearly by defining an exchange flow transport Q_e as the average of Q_{in} and -Q_{out} (recall

293   Q_{out} is defined as negative). We also define an average salinity of the exchange as $\overline{S}$, and the net

294   river flow entering a volume as Q_R (defined as positive).

295
$$Q_e \equiv \frac{(Q_{in} - Q_{out})}{2} \tag{1}$$

296
$$\overline{S} \equiv \frac{(S_{in} + S_{out})}{2} \tag{2}$$

297   Then the tidally averaged, volume-integrated salt budget may be written in two ways:

298
$$\frac{d}{dt} \int S \, dV = Q_{in} S_{in} + Q_{out} S_{out} \tag{3}$$

299
$$\frac{d}{dt} \int S \, dV = -Q_R \overline{S} + Q_e \Delta S \tag{4}$$

300   The terms on the right-hand side of (4) are the TEF equivalent of the classic estuarine salt

301   budget, e.g. Eqn. 10 in MacCready and Geyer (2010), but without the need for a tidal pumping

302   term. Physically, the net river flow removes salt, and the exchange flow brings salt in. The

303   terms in (4) are plotted in Fig. 6c. The gradual decrease of the exchange term, $Q_e \Delta S$, over time

304   is driven by the decrease in stratification, ΔS, but this was more than matched by the decreasing

305   magnitude of the river term, leading to the increase of mean salinity.

306   4.2 Efflux-Reflux Fractions and a Box Model

307   From the time-mean TEF two-layer transports and salinities we may also determine the net

308   vertical mixing in any segment between TEF sections. The method was first developed in

309   Cokelet and Stewart (1985) and was applied to Puget Sound in a series of NOAA reports and one

310   conference paper (Cokelet et al., 1991). What the efflux-reflux formalism does is to split the

10

311   turbulent transport into independent upward and downward components. The advantage of

312   doing so is that it expresses the vertical fluxes as volume transports, making them the vertical

313   equivalent of the horizontal TEF fluxes. The advantage of using the TEF transports is that they

314   are the complete terms which allow (3) to be satisfied, in the same way that they satisfy the

315   Knudsen's relations (Burchard et al., 2018; MacCready, 2011), without the need for fluxes due to

316   tidal pumping, which may not be separated by layer. The existence of realistic numerical

317   simulations, as used here, and the TEF calculation method, represent the main advances in the

318   tools we may use with the efflux-reflux theory. The fact that these tools were not available to

319   Cokelet and Stewart (1985) motivates our effort here to revisit Salish Sea circulation and mixing.

320   Here we extend their method to the entire Salish Sea for multiple years and seasons and use it to

321   construct an efficient box model to calculate residence times for different basins, seasons, and

322   definitions of the residence time (see below). In its simplest form the efflux-reflux theory can be

323   applied to a single channel segment between two sections with no river input (Fig. 7a). The

324   segment is assumed to have two layers and known, steady, volume and salt transports through

325   the open sections on either side. Because of the complexity of applying this to many segments in

326   a complex geometry like the Salish Sea we define a local notation in which all transports are

327   positive, inflows are lower case (q or f) and outflows upper case (Q or F). In standard TEF

328   notation q would be Q_{in}, and f would be $Q_{in}S_{in}$, the inward salt flux. The efflux-reflux theory

329   determines what fraction of the deep (saltier) flow entering the segment must be mixed or

330   advected into the upper (fresher) flow leaving the segment, and this is called "efflux". Likewise,

331   the theory determines what fraction of the fresher flow entering the segment must be mixed or

332   advected down into the saltier flow leaving the segment. The fraction is called "reflux" because

333   in a typical estuarine channel it represents seaward-flowing surface water being mixed down and

334   pulled back landward. The importance of reflux is that it can retain tracers in the system,

335   increasing residence time. The theory determines the efflux-reflux fractions under the dual

336 constraints of volume and salt conservation, as detailed in Cokelet and Stewart (1985). The

337 system of equations to be solved for the segment shown in Fig. 7a are, in matrix form:

338
$$\begin{bmatrix} q_0 & q_1 & 0 & 0 \\ f_0 & f_1 & 0 & 0 \\ 0 & 0 & q_0 & q_1 \\ 0 & 0 & f_0 & f_1 \end{bmatrix} \begin{bmatrix} a_{00} \\ a_{10} \\ a_{01} \\ a_{11} \end{bmatrix} = \begin{bmatrix} Q_0 \\ F_0 \\ Q_1 \\ F_1 \end{bmatrix} \qquad (5)$$

339 The four unknown coefficients, $a_{from,to}$, are then determined by standard matrix techniques. The

340 existence of a solution requires that volume and salt be conserved, e.g. for salt flux:

341
$$f_0 + f_1 = F_0 + F_1 \qquad (6)$$

342 And the fractions must be positive and sum to 1, e.g. $a_{00} + a_{01} = 1$. The efflux and reflux could

343 also be expressed in more familiar form as the sum of vertical advective transport and vertical

344 turbulent transport. Vertical turbulent transport is physically caused by the net effect of upward

345 and downward advection of water parcels, and in the formalism used here we keep track of up

346 and down transports separately.

347 As pointed out at great length by Cokelet and Stewart (1985) there are many real-world

348 complications to applying the theory to complex systems such as the Salish Sea. Chief among

349 these is that for segments with rivers (e.g. W4) or with more than two bounding sections (e.g. J4)

350 the resulting system of equations is underdetermined. For these cases we take a pragmatic,

351 numerical approach, making many guesses for some of the a's and then using the average of all

352 physically possible solutions. In the rare cases with no solutions we impose a typical value of

353 0.1 to the reflux coefficients (a_{00}, a_{11}, and so on). In one segment, A1, we adjusted the reflux

354 fractions by hand to achieve a better result. To ensure exact volume and salt conservation we

355 make very small adjustments (at most 0.5% and usually much smaller) to the fluxes bounding

356 each segment before calculating the fractions. The lack of perfect conservation is due in part to

357 the fact that the volume and salt budgets are not exact, as discussed above. In addition, the net

358 salt in a segment may be changing over time, and this unsteadiness is neglected because it is

359   small compared to the other fluxes. Nonetheless we capture some aspects of temporal variability

360   by calculating the efflux-reflux fractions over different years and seasons.

361   We then use the TEF transports and efflux-reflux fractions to create a box model for arbitrary

362   tracers, as shown schematically in Fig. 7b. Each segment is composed of two volumes, with the

363   upper (fresher) volume being 20% of the total in a given segment – an approximation of the

364   observed structure of the Salish Sea. The residence time results presented below are not

365   particularly sensitive to this choice, varying by only ±7% when the upper volume was 10% or

366   30% of the total in a segment. The concentration of an arbitrary tracer in each volume is given

367   by C, which can be time-dependent even though the circulation is steady. We take all the

368   "reflux" parts of the efflux-reflux calculation and use them to determine upward and downward

369   transports vertically between fresher and saltier volumes in a segment. Following the arrows and

370   notation in Fig. 7b, the equation for tracer concentration in the fresher volume of the segment is:

371

$$\frac{dC_f^{ii}}{dt} = C_f^{iii}q_i + C_s^{ii}q_0a_{00} - C_f^{ii}(Q_0 + q_1a_{11}) \tag{7}$$

372   In segments with more than two surrounding sections the vertical transports are formed by the

373   sum of all the reflux terms. An example of the resulting upward and downward transports for the

374   full year 2017 is plotted in Fig. 8. If they are equal in magnitude that means that there is vertical

375   mixing but no mean vertical flow in a segment. In general, in Fig. 8 it is apparent that upward

376   fluxes are usually larger than downward, implying that the mean transport is upward, consistent

377   with conceptual sketches of estuarine circulation as in MacCready and Geyer (2010) (their Fig.

378   1a). The net up and down transports in each channel are given as text in Fig. 8. Notably, the net

379   upward flow is generally larger than the exchange flow at the seaward end of a channel (see Fig.

380   5) because it must accommodate both the transformation of inflow to outflow and the vertical

381   mixing. Numerically, the box model integrates 37×2 equations such as (7) using forward time-

382   stepping and a time step of one hour (chosen for numerical stability). Had we plotted the

383   transports as vertical velocities (i.e. dividing by the horizontal area of each segment) the sills

384 would show the largest values, but the area integrals in Fig. 8 demonstrate that mixing in basins

385 cannot be neglected.

386 The resulting box model of the Salish Sea can be tested by seeing how well it reproduces the

387 TEF salinities when the boundary conditions are $C = 0$ for all the rivers and $C = S_{in}$ at the two

388 open ocean boundaries. Results of this test for the full year 2017 are plotted in Fig. 9. Overall

389 the box model does a reasonable job of reproducing the along-channel gradient and stratification

390 ($S_{in} - S_{out}$) throughout the system. The model results are biased high in the three channels of

391 Puget Sound, however, and the model underestimates the stratification in Whidbey Basin.

392 Experiments with the box model in an idealized estuary (not shown) suggest that some of the

393 error may be due to the relatively coarse spatial resolution of the boxes. It is also possible that

394 different choices of efflux-reflux fractions in specific segments might improve the model. With

395 its imperfections in mind, we take the box model to be good enough for our purposes of

396 exploring residence times and other properties.

397 We perform two types of experiments with the box model. In the first, we introduce a steady

398 input of tracer with concentration $C = 1$ at a selected river or rivers. We call these "source

399 experiments." The integration is run out to equilibrium (6 years – empirically found to be long

400 enough) and a result consists of the steady-state tracer concentration in each segment, both upper

401 and lower sub-volumes. We also run a tracer with the same boundary conditions but which

402 grows at a known rate, and use the ratio of the two tracers to estimate the "age" of the tracer

403 since it was introduced (e.g. from a river), as discussed for example in Rayson et al. (2016).

404 In the second type of experiment the tracer is introduced as an initial condition with $C = 1$ in a

405 volume V composed of selected segments. We will call these "initial condition experiments."

406 We present results from experiments of this type in seven different basins of the Salish Sea and

407 for different time periods.

408 The concept of residence time has been used in many different ways as discussed for example in

409 Monsen et al. (2002), Delhez et al. (2004) and Lemagie and Lerczak (2015). Usually the

410 motivating question is water quality, e.g. hypoxia, and the time water spends in a region is just

411 one of several driving factors. Residence time is also greatly influenced by how it is defined.

412 Here we adopt the definition that the residence time, T_{res}, is defined through an initial condition

413   experiment: (i) we choose a volume to focus on – e.g. all the water in Puget Sound, (ii) we

414   introduce a conservative tracer with concentration $C = 1$ in that volume at some time, and $C = 0$

415   elsewhere, (iii) we allow advection and mixing to move the tracer around, and then (iv) calculate

416   T_{res} as the time after the start when the integrated tracer concentration in the volume drops to 1/e

417   or about 37% of its original value. We recognize that formally "residence time" is defined for

418   each water parcel (Monsen et al., 2002) and so is a function of space and time. Our T_{res} amounts

419   to an average that describes the behavior of a collection of water parcels, and is analogous to

420   what has variously been called the system residence time, turnover time, or particle tracking

421   timescale.

422   For most of our experiments T_{res} is influenced by reflux: some of the water expelled from a

423   channel by the outgoing branch of the exchange flow may be mixed down outside of the volume

424   under consideration and be returned to the volume by the incoming branch of the exchange flow.

425   The box model described above is an efficient platform for doing such calculations, taking just

426   seconds for a 6-year integration. We may also define an alternate exchange flow, T_{resNX}, which

427   is the "residence time without reflux." It is also calculated from initial condition experiments,

428   but with different rules: instead of allowing the tracer to freely flow and reflux throughout the

429   system, we set $C = 0$ at all times outside of the volume in which the tracer was initialized. A

430   third, and much more common, way to calculate a timescale is as the "flushing time," defined as

431    $T_{flush} = V/Q$ where V is the size of the volume being considered and Q is the water flux through

432   the volume. In our case we take Q to be the sum of all the -Q_{out}, which is equivalent to the sum

433   of all the Q_{in} and the river flows. If the tracer is continuously homogenized within a volume,

434   then it is straightforward to prove that $T_{flush} = T_{resNX}$. However, in general the tracer is not

435   homogenized – some segments of the volume are flushed faster than others, and this lack of

436   homogeneity generally causes $T_{flush} < T_{resNX}$. By calculating all three timescales from our box

437   model experiments we may quantify the relative importance of reflux and lack of

438   homogenization which lead to T_{res} being greater than T_{flush}.

439   We computed TEF transports and vertical efflux-reflux transports for all segments for 15 cases:

440   averages over each of the three years 2017-2019, and the four seasons in each year, defined as

441   averages over three months in a given year: winter = JFM, spring = AMJ, summer = JAS, fall =

442   OND. The transports used in the box model in each case are steady, the result of averaging the

443   full time-varying transports over the time interval in question. When the box model is run for a

444   given case it is different from the real system in the sense that a given circulation pattern and

445   river flow are maintained for much longer than three months or a year, so one can think of the

446   experiments as answering the hypothetical question: what would the residence time be under

447   these conditions if they persisted?

5 Results from the Box Model

449   An example from a source experiment in which the source was all the rivers in the Salish Sea is

450   shown in Fig. 10, with forcing from 2017, a year with average river flow. Notable results are

451   that river water rarely makes up more than 15% of a sub-volume; and only 8% in the main basin

452   of Puget Sound. The age of the water is on the order of 200-300 days, longer in the Strait of

453   Georgia and shorter in Puget Sound. The age represents the combination of transport pathways

454   of many rivers, however, and may be greatly influenced by the system-wide spread of Fraser

455   River water (Banas et al., 2014). The surface concentrations are generally higher (more river

456   influence) and younger.

457   A snapshot from an initial condition experiment is shown in Fig. 11. Here the tracer was

458   initialized in all sub-volumes of South Sound, and then advected and mixed with transports from

459   winter 2019. This was the experiment that had the largest difference between T_{res} and T_{flush}, as

460   discussed below, but it also nicely illustrates the pathways by which a tracer is dispersed

461   throughout the Salish Sea on its way to eventually exiting to the Pacific. In particular, while

462   tracer heads seaward in surface layers, it is also mixed (refluxed) downward, and may thereby

463   drift into other basins, following the deep inflow. This is apparent in all of the channels in Fig.

464   11.

465   Residence times were calculated from initial condition experiments with dye initialized in 7

466   different basins (Fig. 12 and Table 1). Twelve experiments were done in each basin, comprised

467   of three years and four seasons in each year.

468   For the full Salish Sea (all of the segments in Fig. 3a) the average residence time is almost a year

469   and is shortest in summer when the circulation is most affected by the large pulse of freshwater

470   delivered by the Fraser River (Fig. 12). Residence times increased by about 50 days over the

471   three years studied, presumably a result of the weaker river flow in 2019. The flushing time is

472   less than half the residence time, and the difference is due to lack of complete homogenization

473   within the volume. The other possible explanation, reflux, cannot affect this case because the

474   tracer leaving the box model does not come back so $T_{resNX} = T_{res}$ in this case (Fig. 12).

475   Turning to the Strait of Georgia, the residence times are somewhat higher while the flushing

476   times are slightly lower. The longer residence times reflect the fact that deep Strait of Georgia

477   takes a long time to lose its tracer due to its large volume. The effect of reflux is evident in that

478    $T_{resNX} < T_{res}$. From this difference we may calculate the fractional effect of reflux:

$$f_{reflux} = 100 * \frac{(T_{res} - T_{resNX})}{(T_{res} - T_{flush})} \tag{8}$$

480   For this case the average value is $f_{reflux} = 22\%$ (Table 1), meaning that omitting reflux

481   decreases the residence time relative to the flushing time by 22%. From this we may conclude

482   that most (78%) of the reason that $T_{res} > T_{flush}$ is the lack of complete homogenization of tracer

483   in the volume. Physically, much of the tracer is sequestered in parts of the volume that are

484   flushed slowly, while tracer close to the boundaries is flushed very rapidly.

485   The average flushing time in the Strait of Georgia volume is found to be 125 days. This may be

486   compared to estimates made by Rich Pawlowicz et al. (2007). They used time series of

487   observations over three years, exploiting the annual cycle of water properties and the phase lag

488   of properties inside of the Strait of Georgia compared to those of the primary source water in the

489   Strait of Juan de Fuca. Their analysis recognizes the lack of complete homogenization, but they

490   make assumptions consistent with those of the flushing time given above, so their numbers are

491   most directly comparable to our T_{flush}. They examine four layers, the largest of these is the

492   "intermediate layer" (analogous to most of our deep layer) for which they report a flushing time

493   of 160 days. A volume-weighted average of all their layers gives flushing times of 112 days in

494   summer and 172-319 days in winter. The longer times in winter are due to the extreme range (1-

495   3 years) that they give for the flushing time of the deepest water in the Strait of Georgia,

496   although these are never realized because of summer deep renewal events. These bound our

497   estimated average flushing time. Most striking however, is the fact that our mean residence time,

498   379 days, is three times longer than our flushing time, and as discussed above, most of the cause

499   for this increase is lack of homogenization in the volume. Rich Pawlowicz et al. (2007) also

500   estimate that ocean water spends about 1.7 years in the Strait of Georgia after accounting for the

501   substantial reflux in Haro Strait that returns outgoing surface waters back as deep waters. In

502   "source" experiments with our box model (not shown) we find ocean water ages of about 1.2

503   years in the Strait of Georgia. However, there are many different assumptions that go into the

504   two estimates, so they are not exactly comparable. For our results the 50% uncertainty reported

505   in Rich Pawlowicz et al. (2007) is probably a reasonable estimate as well.

506   Similar results are evident in Puget Sound and its basins. Previous median flushing times from

507   D. A. Sutherland et al. (2011) are given in Table 1. These are most directly comparable to the

508   T_{flush} presented here because they used a similar numerical model of the Salish Sea and the Total

509   Exchange Flow method of exchange calculations. The only conceptual difference was that D. A.

510   Sutherland et al. (2011) used the saltwater flushing time whereas we use the volume flushing

511   time; these are very similar for volumes that are mostly seawater. Our results are 14-23% shorter

512   than the previous estimates but display the same pattern among basins: Hood Canal has the

513   longest flushing times, and Whidbey Basin and South Sound are much shorter. As in the Strait

514   of Georgia, the residence times from our box model are markedly longer, being 2-3 or even up to

515   6 times as long as the flushing time. Again, most of the longer time is explained by lack of

516   homogenization within the volume, with only 13-37% explained by reflux (Table 1) in most

517   cases.

518   The exception is the Hood Canal Inner volume which has $f_{reflux} = 83\%$. This experiment

519   differed from the others in that we only initialized tracer in the deeper parts of each segment

520   (H3-H8 in this case). Thus, tracer could be lost rapidly in the no-reflux experiments when it

521   escaped to the upper layer through vertical mixing and advection (i.e. efflux). This result

522   suggests that for a non-conservative tracer which is reset in the upper layer, e.g. by

523   photosynthesis or air-sea gas exchange, the residence time may be closer to the flushing time.

524   **6 Summary and Discussion**

525   In this paper we have presented results from a three-year hindcast of a realistic numerical

526   simulation of the Salish Sea and adjoining coastal waters of the Northeast Pacific. The model is

527   forced with realistic tides, winds, atmospheric heat fluxes, open ocean conditions, and rivers.

528   Based on extensive validation the model is shown to perform well in reproducing observed

529   fields. The model velocity and salinity fields are then used to calculate the exchange flow from

530   hourly snapshots at many sections, using the Total Exchange Flow method. The exchange flow

531   is strongest at the open boundaries, especially the mouth of the Strait of Juan de Fuca, and is

532   amplified by a factor of 20 or more compared to the net river flow. The strength of the exchange

533   flow decreases gradually, and nearly monotonically, going landward. This implies that the many

534   basins of the Salish Sea are intrinsically connected to each other by this exchange flow.

535   The vertical mixing throughout the system was quantified using the efflux-reflux method of

536   Cokelet and Stewart (1985). In this formalism vertical mixing and advection are expressed as

537   opposing upward and downward volume fluxes, analogous to the horizontal TEF fluxes.

538   Notably the downward fluxes highlight the many places where the outward flowing surface layer

539   is refluxed into the landward-flowing deep layer, fundamentally shaping the tracer transport

540   pathways. Low river flow in 2019 resulted in a clear increase of salinity in Puget Sound, and a

541   decrease in stratification, but no obvious change to the exchange flow. Nevertheless, residence

542   times were longer in 2019 compared to 2017-8. A box model for tracer transport was developed

543   using these horizontal and vertical fluxes, with transports from four seasons in each of three

544   years. The box model allowed rapid calculation of residence times for a number of sub-volumes.

545   In general, it was found that the tracer-based residence time from the box model was often a

546   factor of two longer than the more traditional calculation of flushing time. The increase was due

547   in part to refluxing which brings tracer back into a volume, but in larger measure the increase

548   was due to the fact that tracer was not mixed uniformly throughout a volume. The fact that

549   timescales for water renewal could be a factor of 2-3 different depending on the method of

550   estimation used means we should be cautious in interpreting the "residence time." Based on

551   results here we may conclude that the *relative* timescales among basins are reasonably well

552   determined by all methods, but the actual values of the timescales requires consideration of other

553   factors that may influence a specific tracer, as for example the effects on hypoxia of

554   photosynthesis, air-sea gas exchange, and water column and benthic rates of the remineralization

555   of sinking organic matter.

556   There are a number of limitations of the box model presented here that should be kept in mind.

557   It is only as accurate as the LiveOcean transports used to create it, and these are hard to validate

558   directly because of the relative lack of current meter data. There is uncertainty in the estimation

559   of reflux coefficients, and in the translation of those to the box model. The box model assumes

560   static forcing over a season and so cannot capture events like large pulses of river flow. Finally,

561   the number of segments chosen can influence the results. For example, the flushing times are

562   essentially like the no-reflux residence times in the limit of a single box instead of many

563   segments and two layers, and the results in Fig. 12 and Table 1 clearly show that adding more

564   boxes increases residence time by resolving regions with slower flushing. It is an open question

565   whether or not adding more segments would significantly increase the residence time further.

566   Pursuing this line of reason leads to the conclusion that detailed problems are better studied with

567   the full model, whereas the box model excels as a very fast tool for initial estimation and

568   understanding.

569   While this paper focuses largely on the economically and ecologically important Salish Sea, the

570   methods and results are applicable across all estuaries. The combined use of TEF with

571   efflux/reflux is a valuable approach likely to prove fruitful in other systems. Moreover, the

572   importance of considering efflux/reflux and incomplete tracer homogenization are expected to be

573   critical to understanding residence times in many estuaries.

589 All code used in the analysis is available at https://github.com/parkermac/LiveOcean.git, in

590 particular in the x_tef folder. Model input parameters are in the folder

591 forcing/dot_in/cas6_v3_lo8b. The TEF section extractions and processed files required to run

592 the box model are archived and freely available here (start with the README.txt in the folder

593 after extraction):

594 https://pm2.blob.core.windows.net/pm-share/LO_TEF_data_2020_11.tar.gz.

595 [references from the supplement: (Babson et al., 2006) (Brasseale et al., 2019) (Codiga, 2011)

596 (Davis et al., 2014) (Egbert & Erofeeva, 2002) (Emery & Thomson, 1998) (Feely et al., 2016)

597 (Finlayson, 2005) (Foreman et al., 1995) (Fredrickson et al., 2019) (Giddings & MacCready,

598 2017) (Giddings et al., 2014) (Haidvogel et al., 2000) (Khangaonkar et al., 2017) (Lavelle et al.,

599 1988) (Liu et al., 2009) (Mass et al., 2003) (Metzger et al., 2014) (Mohamedali et al., 2011)

600 (Shchepetkin & McWilliams, 2005) (Siedlecki et al., 2015) (D. A. Sutherland et al., 2011) (G.

601 Sutherland et al., 2005) (Richard E Thomson & Huggett, 1980) (Tozer et al., 2019)]

References

603

604 Babson, A. L., Kawase, M., & MacCready, P. (2006). Seasonal and Interannual Variability in the
605   Circulation of Puget Sound, Washington: A Box Model Study. *Atmosphere-Ocean, 44*,
606   29-45. doi:10.3137/ao.440103
607 Banas, N. S., Conway-Cranos, L., Sutherland, D. A., MacCready, P., Kiffney, P., & Plummer,
608   M. (2014). Patterns of River Influence and Connectivity Among Subbasins of Puget
609   Sound, with Application to Bacterial and Nutrient Loading. *Estuaries and Coasts, 38*(3),
610   735-753. doi:10.1007/s12237-014-9853-y
611 Brasseale, E., Grason, E. W., McDonald, P. S., Adams, J., & MacCready, P. (2019). Larval
612   Transport Modeling Support for Identifying Population Sources of European Green Crab
613   in the Salish Sea. *Estuaries and Coasts*. doi:10.1007/s12237-019-00586-2
614 Bretschneider, D. E., Cannon, G. A., Holbrook, J. R., & Pashinski, D. J. (1985). Variability of
615   Subtidal Current Structure in a Fjord Estuary: Puget Sound, Washington. *Journal of
616   Geophysical Research, 90*, 11,949-911,958. doi:10.1029/JC090iC06p11949
617 Burchard, H., Bolding, K., Feistel, R., Gräwe, U., Klingbeil, K., MacCready, P., et al. (2018).
618   The Knudsen theorem and the Total Exchange Flow analysis framework applied to the
619   Baltic Sea. *Progress in Oceanography, 165*, 268-286. doi:10.1016/j.pocean.2018.04.004
620 Chen, S.-N., Geyer, W. R., Ralston, D. K., & Lerczak, J. A. (2012). Estuarine Exchange Flow
621   Quantified with Isohaline Coordinates: Contrasting Long and Short Estuaries. *Journal of
622   Physical Oceanography, 42*(5), 748-763. doi:10.1175/jpo-d-11-086.1
623 Codiga, D. L. (2011). *Unified Tidal Analysis and Prediction Using the UTide Matlab Functions*.
624   Retrieved from ftp://www.po.gso.uri.edu/pub/downloads/codiga/pubs/2011Codiga-
625   UTide-Report.pdf

626   Cokelet, E. D., & Stewart, R. J. (1985). The exchange of water in fjords: The efflux/reflux theory
627   of advective reaches separated by mixing zones. *Journal of Geophysical Research,*
628   *90*(C4), 7287-7306. doi:10.1029/JC090iC04p07287
629   Cokelet, E. D., Stewart, R. J., & Ebbesmeyer, C. C. (1991). *Concentrations and ages of*
630   *conservative pollutants in Puget Sound.* Paper presented at the Puget Sound Research
631   '91.
632   Collias, E., McGary, N., & Barnes, C. A. (1974). *Atlas of physical and chemical properties of*
633   *Puget Sound and its surrounding approaches*. Retrieved from
634   Conroy, T., Sutherland, D. A., & Ralston, D. K. (2020). Estuarine Exchange Flow Variability in
635   a Seasonal, Segmented Estuary. *Journal of Physical Oceanography, 50*(3), 595-613.
636   doi:10.1175/jpo-d-19-0108.1
637   Crean, P. B., & Ages, A. B. (1971). *Oceanographic records from twelve cruises in the Strait of*
638   *Georgia and Juan de Fuca Strait, 1968*. Retrieved from
639   Davis, K. A., Banas, N. S., Giddings, S. N., Siedlecki, S. A., MacCready, P., Lessard, E. J., et al.
640   (2014). Estuary-enhanced upwelling of marine nutrients fuels coastal productivity in the
641   U.S. Pacific Northwest. *Journal of Geophysical Research: Oceans, 119*(12), 8778-8799.
642   doi:10.1002/2014jc010248
643   Delhez, É. J. M., Heemink, A. W., & Deleersnijder, É. (2004). Residence time in a semi-
644   enclosed domain from the solution of an adjoint problem. *Estuarine, Coastal and Shelf*
645   *Science, 61*(4), 691-702. doi:10.1016/j.ecss.2004.07.013
646   Deppe, R. W., Thomson, J., Polagye, B., & Krembs, C. (2018). Predicting Deep Water Intrusions
647   to Puget Sound, WA (USA), and the Seasonal Modulation of Dissolved Oxygen.
648   *Estuaries and Coasts, 41*, 114-127. doi:10.1007/s12237-017-0274-6
649   Ebbesmeyer, C. C., & Barnes, C. A. (1980). Control of a fjord basin's dynamics by tidal mixing
650   in embracing sill zones. *Estuarine and Coastal Marine Science, 11*, 311-330.
651   doi:10.1016/S0302-3524(80)80086-7
652   Ebbesmeyer, C. C., Word, J. Q., & Barnes, C. A. (1988). Puget Sound: A Fjord System
653   Homogenized with Water Recycled over Sills by Tidal Mixing. In *Hydrodynamics of*
654   *Estuaries: Volume II* (pp. 17-29).
655   Egbert, G. D., & Erofeeva, S. Y. (2002). Efficient inverse modeling of barotropic ocean tides.
656   *Journal of Atmospheric and Oceanic Technology, 19*, 183-204. doi:10.1175/1520-
657   0426(2002)019<0183:EIMOBO>2.0.CO;2
658   Emery, W. J., & Thomson, R. E. (1998). *Data Analysis Methods in Physical Oceanography*.
659   Kidlington, Oxford: Elsevier Science.
660   Feely, R. A., Alin, S. R., Carter, B., Bednaršek, N., Hales, B., Chan, F., et al. (2016). Chemical
661   and biological impacts of ocean acidification along the west coast of North America.
662   *Estuarine, Coastal and Shelf Science, 183*, 260-270. doi:10.1016/j.ecss.2016.08.043
663   Finlayson, D. P. (2005). *Combined bathymetry and topography of the Puget Lowland,*
664   *Washington State*. Retrieved from
665   https://www.ocean.washington.edu/data/pugetsound/psdem2005.html
666   Foreman, M. G. G., Walters, R. A., Henry, R. F., Keller, C. P., & Dolling, A. G. (1995). A tidal
667   model for eastern Juan de Fuca Strait and the southern Strait of Georgia. *J. Geophys.*
668   *Res., 100*, 721-740. doi:10.1029/94JC02721
669   Fredrickson, E. K., Wilcock, W. S. D., Schmidt, D. A., MacCready, P., Roland, E., Kurapov, A.
670   L., et al. (2019). Optimizing Sensor Configurations for the Detection of Slow-Slip
671   Earthquakes in Seafloor Pressure Records, Using the Cascadia Subduction Zone as a

672   Case Study. *Journal of Geophysical Research: Solid Earth, 124*, 13504-13531.
673   doi:10.1029/2019JB018053
674 Geyer, W. R., & Cannon, G. A. (1982). Sill processes related to deep water renewal in a fjord.
675   *Journal of Geophysical Research, 87*, 7985. doi:10.1029/JC087iC10p07985
676 Geyer, W. R., & MacCready, P. (2014). The Estuarine Circulation. *Annual Review of Fluid*
677   *Mechanics, 46*, 175-197. doi:10.1146/annurev-fluid-010313-141302
678 Giddings, S. N., & MacCready, P. (2017). Reverse Estuarine Circulation Due to Local and
679   Remote Wind Forcing, Enhanced by the Presence of Along-Coast Estuaries. *Journal of*
680   *Geophysical Research: Oceans, 122*, 10184-10205. doi:10.1002/2016JC012479
681 Giddings, S. N., MacCready, P., Hickey, B. M., Banas, N. S., Davis, K. A., Siedlecki, S. A., et
682   al. (2014). Hindcasts of potential harmful algal bloom transport pathways on the Pacific
683   Northwest coast. *Journal of Geophysical Research: Oceans, 119*, 2439-2461.
684   doi:10.1002/2013JC009622
685 Gregg, M. C., & Pratt, L. J. (2010). Flow and Hydraulics near the Sill of Hood Canal, a Strongly
686   Sheared, Continuously Stratified Fjord. *Journal of Physical Oceanography, 40*, 1087-
687   1105. doi:10.1175/2010JPO4312.1
688 Hagy, J. D., Boynton, W. R., & Sanford, L. P. (2000). Estimation of Net Physical Transport and
689   Hydraulic Residence Times for a Coastal Plain Estuary Using Box Models. *Estuaries, 23*,
690   328-340. doi:10.2307/1353325
691 Haidvogel, D. B., Arango, H. G., Hedstrom, K., Beckmann, A., Malanotte-Rizzoli, P., &
692   Shchepetkin, A. F. (2000). Model evaluation experiments in the North Atlantic Basin:
693   simulations in nonlinear terrain-following coordinates. *Dynamics of Atmospheres and*
694   *Oceans, 32*, 239-281. doi:10.1016/S0377-0265(00)00049-X
695 Hansen, D. V., & Rattray, M., Jr . (1965). Gravitational circulation in straits and estuaries.
696   *Journal of Marine Research, 23*, 104-122.
697 Khangaonkar, T., Long, W., & Xu, W. (2017). Assessment of circulation and inter-basin
698   transport in the Salish Sea including Johnstone Strait and Discovery Islands pathways.
699   *Ocean Modelling, 109*, 11-32. doi:10.1016/j.ocemod.2016.11.004
700 Khangaonkar, T., Yang, Z., Kim, T., & Roberts, M. (2011). Tidally averaged circulation in Puget
701   Sound sub-basins: Comparison of historical data, analytical model, and numerical model.
702   *Estuarine, Coastal and Shelf Science, 93*, 305-319. doi:10.1016/j.ecss.2011.04.016
703 Knudsen, M. (1900). Ein hydrographischer Lehrsatz. *Ann. Hydrogr. Mar. Meterol., 28*, 316-320.
704 Lavelle, J. W., Mofjeld, H. O., Lempriere-Doggett, E., Cannon, G. A., Pashinski, D. J., Cokelet,
705   E. D., et al. (1988). *A multiply-connected channel model of tides and tidal currents in*
706   *Puget Sound, Washington and a comparison with updated observations*. Retrieved from
707   https://www.pmel.noaa.gov/pubs/PDF/lave967/lave967.pdf
708 LeBlond, P. H. (1983). The Strait of Georgia: functional anatomy of a coastal sea. *Canadian*
709   *Journal of Fisheries and Aquatic Sciences, 40*, 1033-1063. doi:10.1139/f83-128
710 Lemagie, E. P., & Lerczak, J. A. (2015). A Comparison of Bulk Estuarine Turnover Timescales
711   to Particle Tracking Timescales Using a Model of the Yaquina Bay Estuary. *Estuaries*
712   *and Coasts, 38*, 1797-1814. doi:10.1007/s12237-014-9915-1
713 Li, M., Gargett, A., & Denman, K. (1999). Seasonal and internannual variability of estuarine
714   circulation in a box model of the Strait of Georgia and Juan de Fuca strait. *Atmosphere-*
715   *Ocean, 37*, 1-19. doi:10.1080/07055900.1999.9649619

716 Liu, Y., MacCready, P., Hickey, B. M., Dever, E. P., Kosro, P. M., & Banas, N. S. (2009).
717   Evaluation of a coastal ocean circulation model for the Columbia River plume in summer
718   2004. *Journal of Geophysical Research, 114*. doi:10.1029/2008jc004929
719 Lorenz, M., Klingbeil, K., & Burchard, H. (2020). Numerical Study of the Exchange Flow of the
720   Persian Gulf Using an Extended Total Exchange Flow Analysis Framework. *Journal of
721   Geophysical Research: Oceans, 125*(2). doi:10.1029/2019jc015527
722 Lorenz, M., Klingbeil, K., MacCready, P., & Burchard, H. (2019). Numerical issues of the Total
723   Exchange Flow (TEF) analysis framework for quantifying estuarine circulation. *Ocean
724   Science Discussions*, 1-21. doi:10.5194/os-2018-147
725 MacCready, P. (2011). Calculating Estuarine Exchange Flow Using Isohaline Coordinates.
726   *Journal of Physical Oceanography, 41*, 1116-1124. doi:10.1175/2011JPO4517.1
727 MacCready, P., & Geyer, W. R. (2010). Advances in Estuarine Physics. *Annual Review of
728   Marine Science, 2*, 35-58. doi:10.1146/annurev-marine-120308-081015
729 MacCready, P., Geyer, W. R., & Burchard, H. (2018). Estuarine Exchange Flow Is Related to
730   Mixing through the Salinity Variance Budget. *Journal of Physical Oceanography, 48*,
731   1375-1384. doi:10.1175/JPO-D-17-0266.1
732 Mass, C. F., Albright, M., Ovens, D., Steed, R., MacIver, M., Grimit, E., et al. (2003). Regional
733   environmental prediction over the Pacific Northwest. *Bulletin of the American
734   Meteorological Society, 84*, 1353-1366+1328. doi:10.1175/BAMS-84-10-1353
735 Masson, D., & Peña, A. (2009). Chlorophyll distribution in a temperate estuary: The Strait of
736   Georgia and Juan de Fuca Strait. *Estuarine, Coastal and Shelf Science, 82*(1), 19-28.
737   doi:10.1016/j.ecss.2008.12.022
738 Metzger, E. J., Smedstad, O. M., Thoppil, P., Hurlburt, H., Cummings, J., Walcraft, A., et al.
739   (2014). US Navy Operational Global Ocean and Arctic Ice Prediction Systems.
740   *Oceanography, 27*(3), 32-43. doi:10.5670/oceanog.2014.66
741 Mofjeld, H. O., & Larsen, L. H. (1984). *Tides and tidal currents of the inland waters of Western
742   Washington*. Retrieved from https://www.pmel.noaa.gov/pubs/PDF/mofj687/mofj687.pdf
743 Mohamedali, T., Roberts, M., Sackmann, B., Whiley, A., & Kolosseus, A. (2011). *South Puget
744   Sound Dissolved Oxygen Study Interim Nutrient Load Summary for 2006-2007*
745   (8778336341). Retrieved from
746 Monsen, N. E., Cloern, J. E., Lucas, L. V., & Monismith, S. G. (2002). A comment on the use of
747   flushing time, residence time, and age as transport time scales. *Limnology and
748   Oceanography, 47*(5), 1545-1553. doi:10.4319/lo.2002.47.5.1545
749 Moore, S. K., Johnstone, J. A., Banas, N. S., & Salathe, E. P., Jr. (2015). Present-day and future
750   climate pathways affecting Alexandrium blooms in Puget Sound, WA, USA. *Harmful
751   Algae, 48*, 1-11. doi:10.1016/j.hal.2015.06.008
752 Olson, E. M., Allen, S. E., Do, V., Dunphy, M., & Ianson, D. (2020). Assessment of Nutrient
753   Supply by a Tidal Jet in the Northern Strait of Georgia Based on a Biogeochemical
754   Model. *Journal of Geophysical Research: Oceans, 125*(8). doi:10.1029/2019jc015766
755 Pawlowicz, R. (2001). A Tracer Method for Determining Transport in Two-Layer Systems,
756   Applied to the Strait of Georgia/Haro Strait/Juan de Fuca Strait Estuarine System.
757   *Estuarine, Coastal and Shelf Science, 52*(4), 491-503. doi:10.1006/ecss.2000.0748
758 Pawlowicz, R., Riche, O., & Halverson, M. (2007). The circulation and residence time of the
759   strait of Georgia using a simple mixing-box approach. *Atmosphere-Ocean, 45*, 173-193.
760   doi:10.3137/ao.450401

761   Peña, M. A., Masson, D., & Callendar, W. (2016). Annual plankton dynamics in a coupled
762   physical–biological model of the Strait of Georgia, British Columbia. *Progress in*
763   *Oceanography, 146*, 58-74. doi:10.1016/j.pocean.2016.06.002

764   Pinardi, N., Cessi, P., Borile, F., & Wolfe, C. L. P. (2019). The Mediterranean Sea Overturning
765   Circulation. *Journal of Physical Oceanography, 49*, 1699-1721. doi:10.1175/JPO-D-18-
766   0254.1

767   Ralston, D. K., Geyer, W. R., & Lerczak, J. A. (2008). Subtidal Salinity and Velocity in the
768   Hudson River Estuary: Observations and Modeling. *Journal of Physical Oceanography,*
769   *38*, 753-770. doi:10.1175/2007JPO3808.1

770   Rayson, M. D., Gross, E. S., Hetland, R. D., & Fringer, O. B. (2016). Time scales in Galveston
771   Bay: An unsteady estuary. *Journal of Geophysical Research: Oceans, 121*, 2268-2285.
772   doi:10.1002/2015JC011181

773   Rayson, M. D., Gross, E. S., Hetland, R. D., & Fringer, O. B. (2017). Using an Isohaline Flux
774   Analysis to Predict the Salt Content in an Unsteady Estuary. *Journal of Physical*
775   *Oceanography, 47*, 2811-2828. doi:10.1175/JPO-D-16-0134.1

776   Riche, O., Johannessen, S. C., & Macdonald, R. W. (2014). Why timing matters in a coastal sea:
777   Trends, variability and tipping points in the Strait of Georgia, Canada. *Journal of Marine*
778   *Systems, 131*, 36-53. doi:10.1016/j.jmarsys.2013.11.003

779   Seim, H. E., & Gregg, M. C. (1994). Detailed observations of a naturally occurring shear
780   instability. *Journal of Geophysical Research, 99*, 10049. doi:10.1029/94JC00168

781   Shchepetkin, A. F., & McWilliams, J. C. (2005). The regional oceanic modeling system
782   (ROMS): a split-explicit, free-surface, topography-following-coordinate oceanic model.
783   *Ocean Modelling, 9*, 347-404. doi:10.1016/j.ocemod.2004.08.002

784   Siedlecki, S. A., Banas, N. S., Davis, K. A., Giddings, S. N., Hickey, B. M., MacCready, P., et
785   al. (2015). Seasonal and interannual oxygen variability on the Washington and Oregon
786   continental shelves. *Journal of Geophysical Research: Oceans, 120*(2), 608-633.
787   doi:10.1002/2014jc010254

788   Soontiens, N., Allen, S. E., Latornell, D., Le Souëf, K., Machuca, I., Paquin, J.-P., et al. (2015).
789   Storm Surges in the Strait of Georgia Simulated with a Regional Model. *Atmosphere-*
790   *Ocean, 54*(1), 1-21. doi:10.1080/07055900.2015.1108899

791   Sutherland, D. A., MacCready, P., Banas, N. S., & Smedstad, L. F. (2011). A Model Study of the
792   Salish Sea Estuarine Circulation. *Journal of Physical Oceanography, 41*(6), 1125-1143.
793   doi:10.1175/2011jpo4540.1

794   Sutherland, G., Garrett, C., & Foreman, M. (2005). Tidal Resonance in Juan de Fuca Strait and
795   the Strait of Georgia. *Journal of Physical Oceanography, 35*(7), 1279-1286.
796   doi:10.1175/jpo2738.1

797   Thomson, R. E., & Huggett, W. S. (1980). M2 Baroclinic Tides in Johnstone Strait, British
798   Columbia. *Journal of Physical Oceanography, 10*, 1509-1539. doi:10.1175/1520-
799   0485(1980)010<1509:MBTIJS>2.0.CO;2

800   Thomson, R. E., Mihály, S. F., & Kulikov, E. A. (2007). Estuarine versus transient flow regimes
801   in Juan de Fuca Strait. *Journal of Geophysical Research: Oceans, 112*, 1-25.
802   doi:10.1029/2006JC003925

803   Thyng, K. M., Hetland, R. D., Zimmerle, H. M., & DiMarco, S. F. (2016). True colors of
804   oceanography: Guidelines for effective and accurate colormap selection. *Oceanography*,
805   9-13. doi:10.5670/oceanog.2016.66

806   Tozer, B., Sandwell, D. T., Smith, W. H. F., Olson, C., Beale, J. R., & Wessel, P. (2019). Global
807   Bathymetry and Topography at 15 Arc Sec: SRTM15+. *Earth and Space Science, 6*(10),
808   1847-1864. doi:10.1029/2019ea000658

809

810
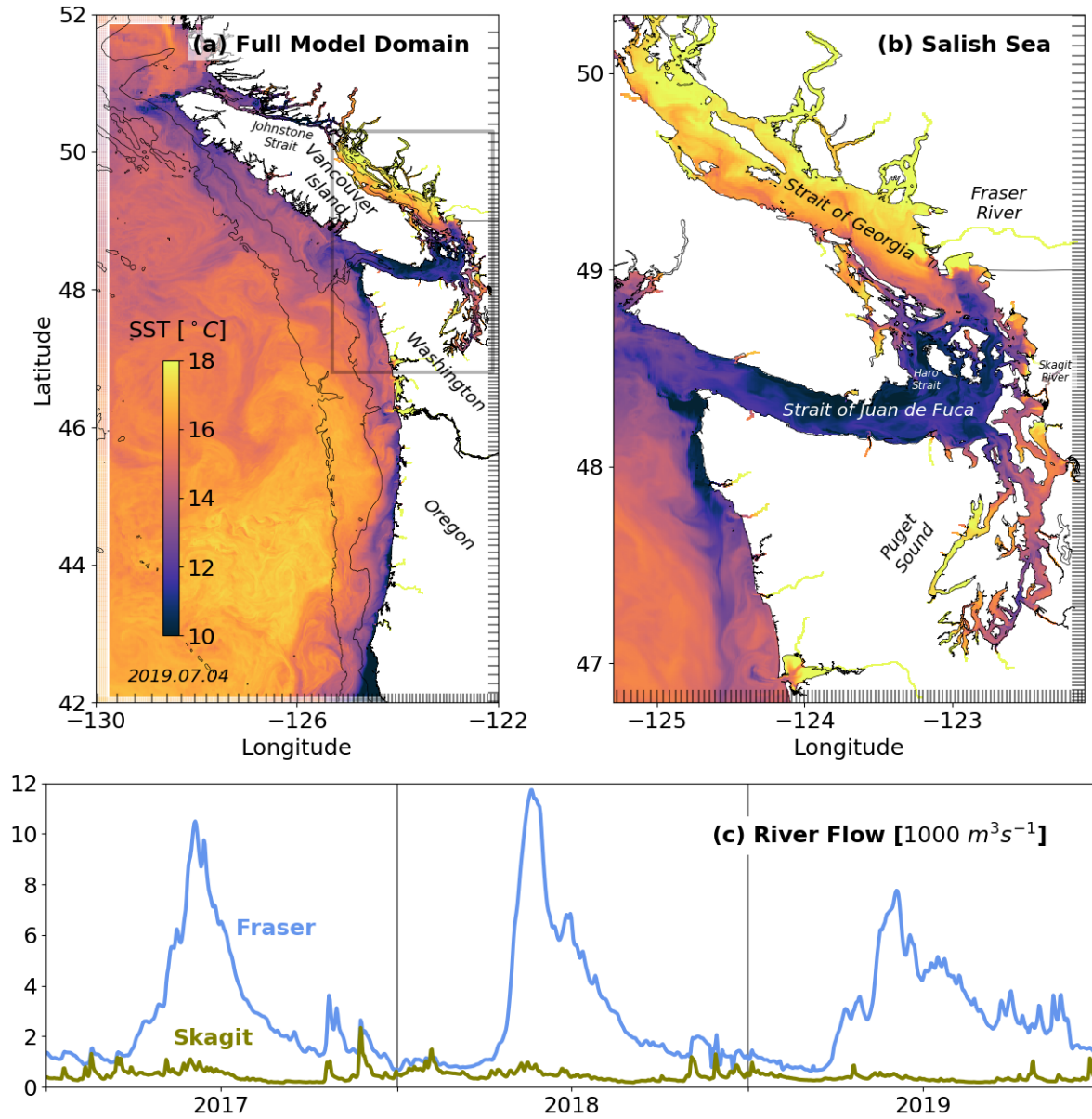
Figure 1. LiveOcean model domain (a) colored by sea surface temperature for July 4, 2019. Grid spacing is indicated with tick marks (only every 10th grid point is drawn). Region of nudging to climatology at open boundaries is indicated by transparency. Bathymetry contours for 200 m and 2000 m are plotted as black lines. Close up of the model (b) for the Salish Sea with ticks for every 4th grid point. Three-year time series (c) of flow in the Fraser and Skagit Rivers, year is labeled at the middle of the year.
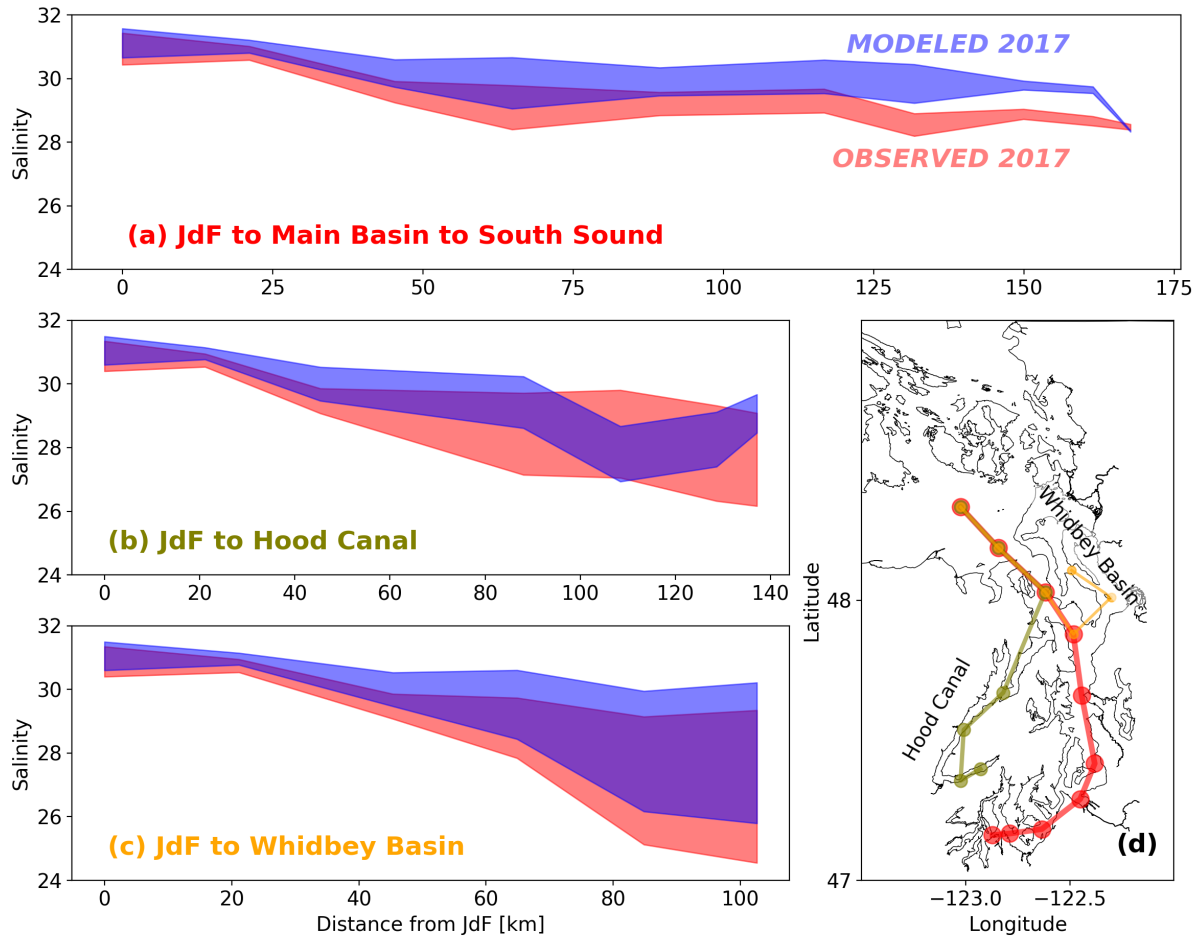
Figure 2. Along-channel salinity distribution calculated from 2017 annual-average salinity using monthly CTD casts (OBSERVED: red) and corresponding model fields (MODELED: blue). The vertical thickness of each line expresses the average stratification: the upper and lower limits are the salinity averaged below and above a chosen depth. The section down Main Basin (a) used 20 m for the chosen depth, while (b) and (c) used 10 m because Hood Canal and Whidbey Basin are more strongly stratified than Main Basin. Station locations are plotted in (d). The colored lines in (d) are the transects shown in (a)-(c).

831
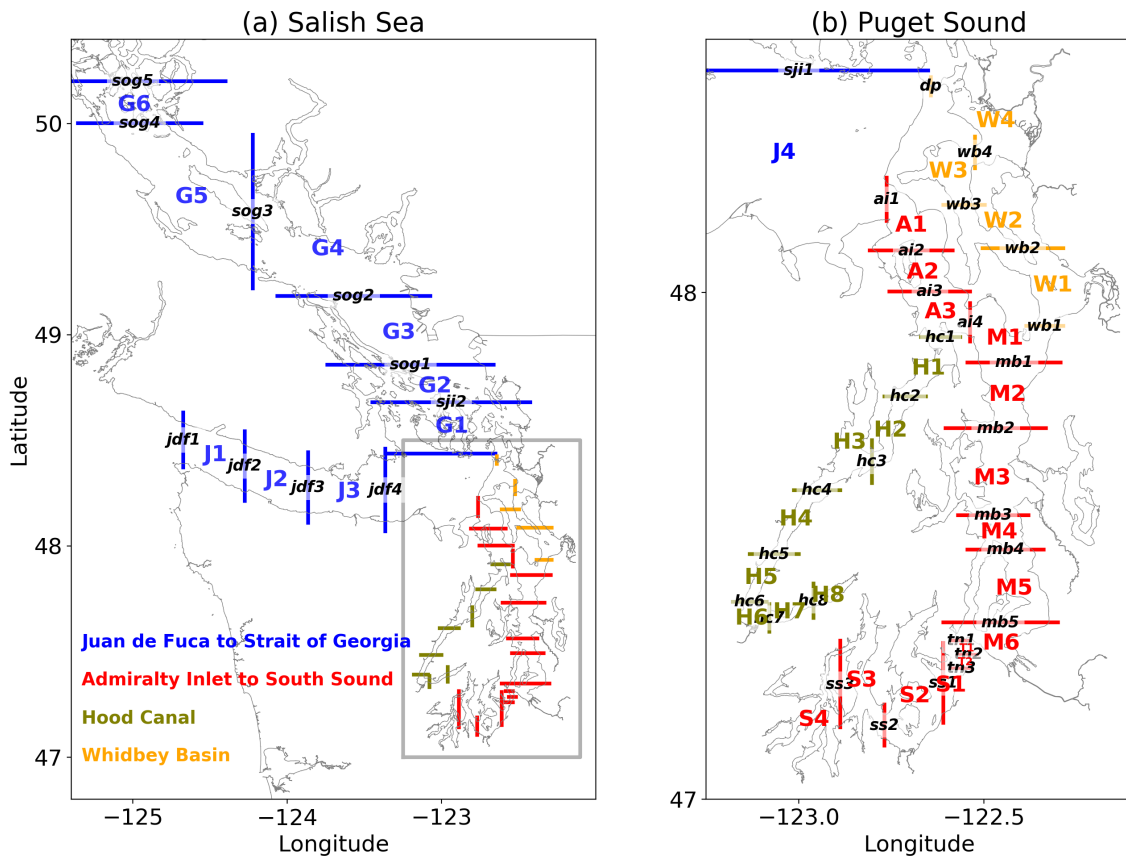
832

833

834 Figure 3. Sections used for the Total Exchange Flow analysis in the Salish Sea (a). Sections are

835 shown as lines and lower-case names like *jdf1*. A close up of Puget Sound sections is shown in

836 (b). The names of segments (the volumes in-between sections) such as J1 are also shown.

837 Segment letters denote the following basins or sills in Puget Sound (b): A = Admiralty Inlet, M =

838 Main Basin, T = Tacoma Narrows, S = South Sound, H = Hood Canal, W = Whidbey Basin. In

839 the larger Salish Sea (a) J = Strait of Juan de Fuca, G = Strait of Georgia. Section *sog5* at the top

840 of (a) is the start of Johnstone Strait which is a minor connection between the Strait of Georgia

841 and the Pacific Ocean. Section *dp* near the top of (b) is Deception Pass which connects the north

842 end of Whidbey Basin to the eastern Strait of Juan de Fuca. The sections *tn1*, *tn2*, and *tn3* in (b)

843 are at Tacoma Narrows which connects South Sound to Main Basin.

844
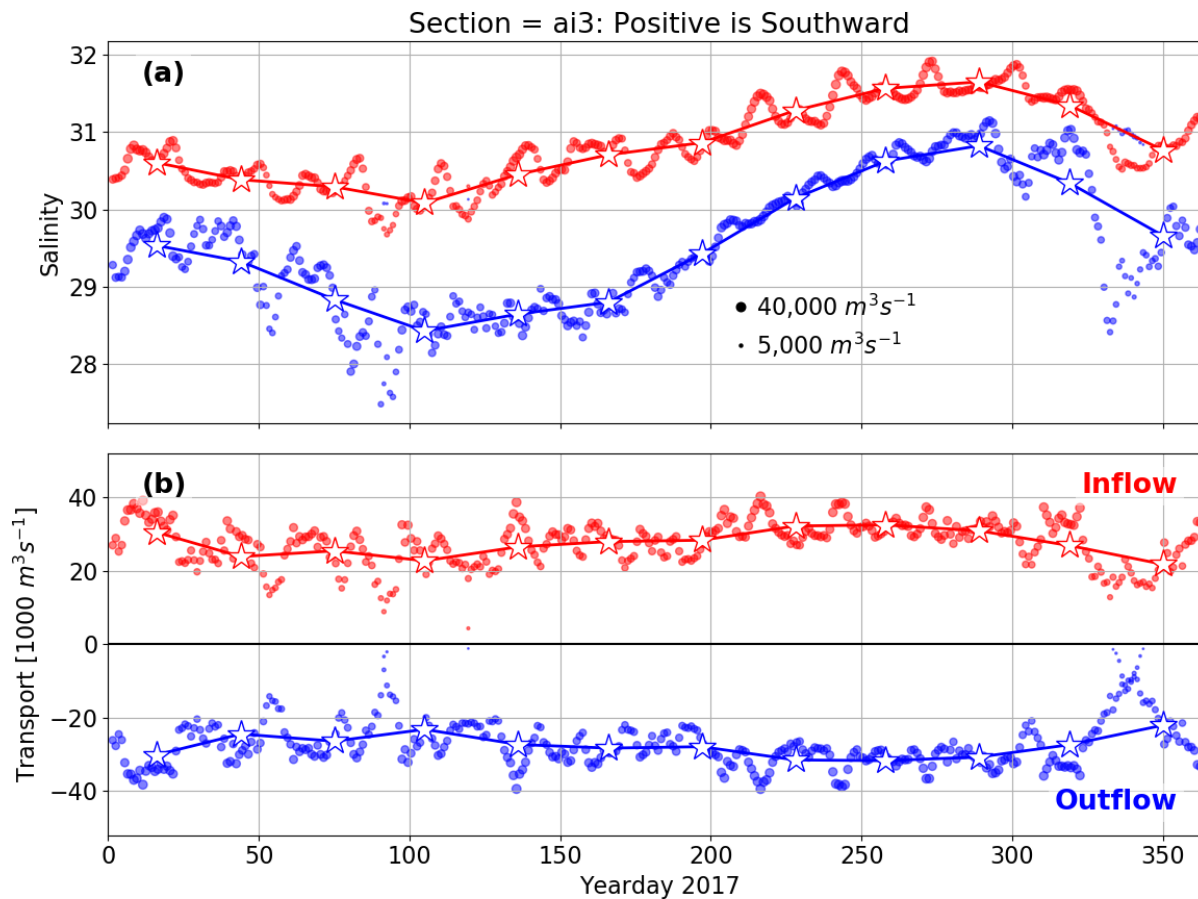
Figure 4. Total Exchange Flow salinity (a) and transport (b) at section *ai3* in Admiralty Inlet plotted vs. yearday for 2017. The red and blue dots show tidally averaged daily salinity or transport from the multi-layer TEF analysis. Dot size is proportional to transport. The monthly averaged two-layer TEF terms S_{in}, S_{out} and Q_{in}, Q_{out} are shown as stars connected by lines.
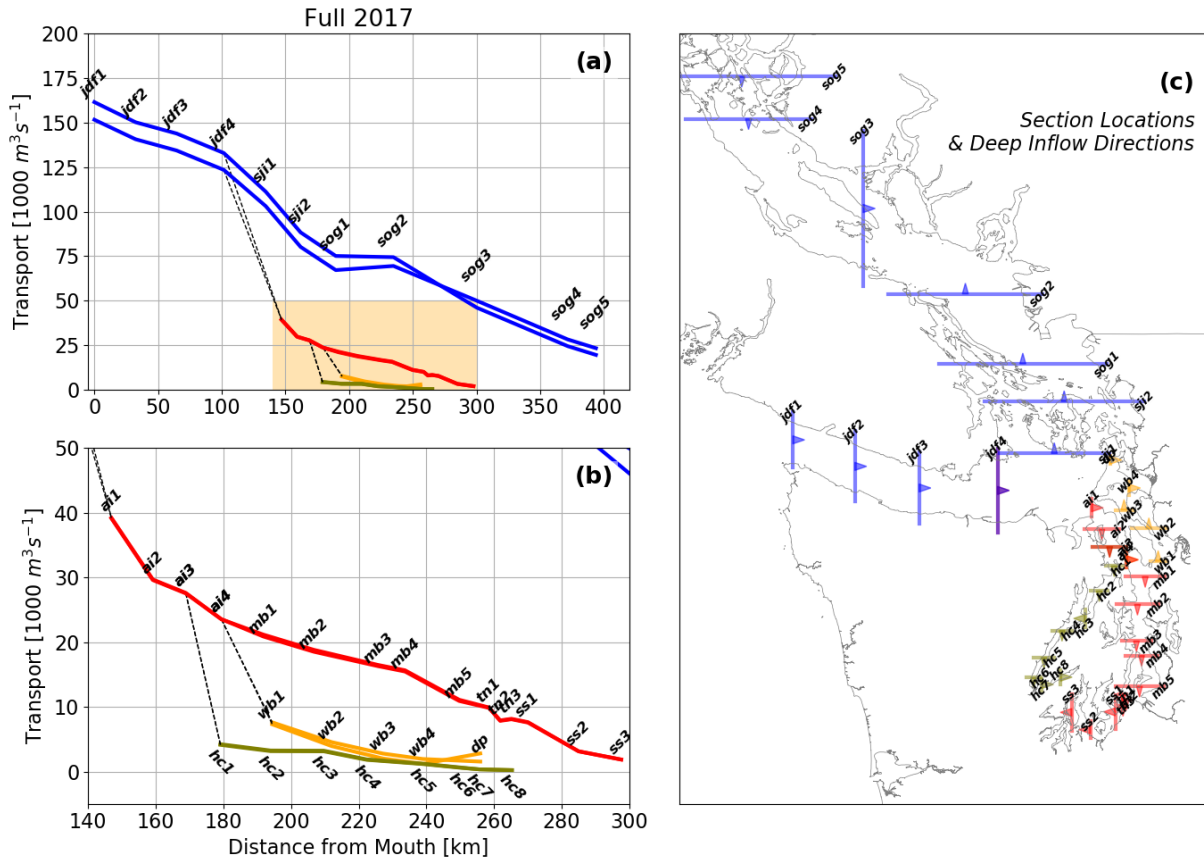
Figure 5. Total Exchange Flow volume transports averaged over 2017 for the four main channels of the Salish Sea (a). The lines are Q_{in} and $-Q_{out}$, so the higher of the two blue lines in (a) is the outflow. An expanded view of Puget Sound transports is plotted in (b). Section locations and names are shown in (c) with the spike on each section line showing the direction of the deep inflow. Note that the exchange flow reverses sign in the Strait of Georgia between sections *sog2* and *sog3*. The dashed lines at the seaward end of basins, e.g. from *hc1* to *ai3* in (b) indicate connections between the channels.
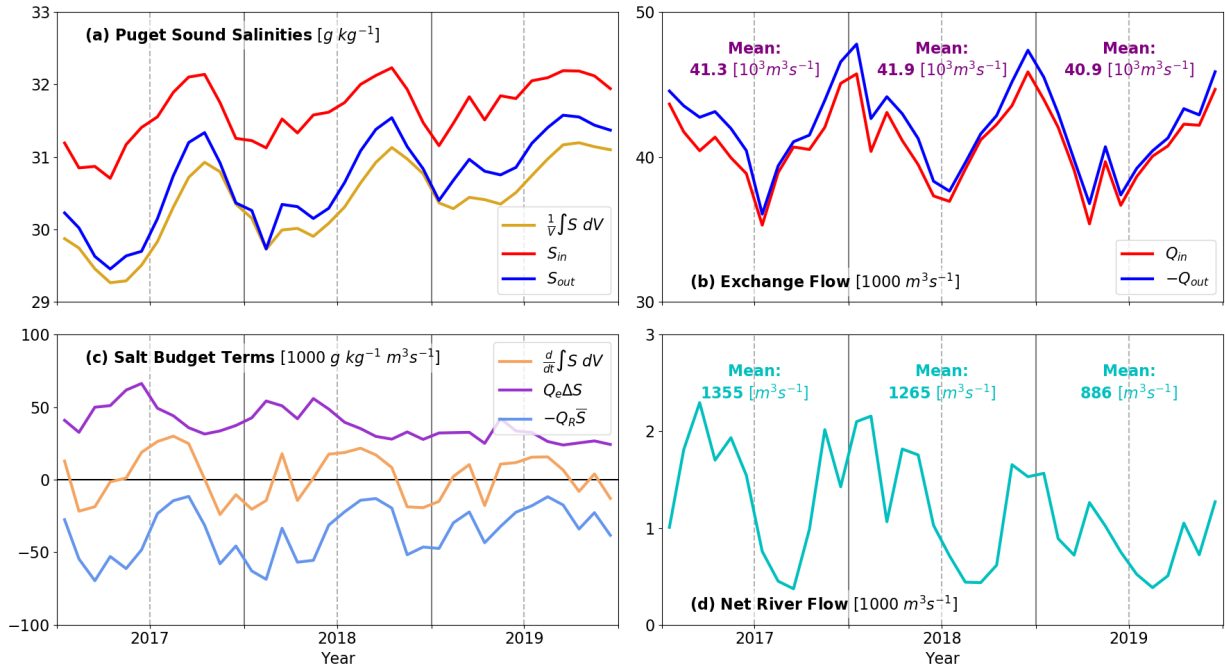
Figure 6. Three-year TEF analysis time series for Puget Sound salinity. The bounding sections for the volume are *ai1* and *dp*. Salinities of the in- and outflow are plotted in (a) along with the mean salinity in the volume. The term $V^{-1} \int S \, dV$ is lower than S_{in} and S_{out} because is it the average over the whole volume of Puget Sound, not the average of S_{in} and S_{out}. All values are monthly averages. The exchange flow transports are plotted in (b) with annual means shown for each year as text. Terms in the exchange flow salt budget are plotted in (c). The net river flow is plotted in (d) with annual means shown for each year as text. Year labels are at the middle of the year.

(a) Efflux-Reflux Notation

(b) Box Model Notation
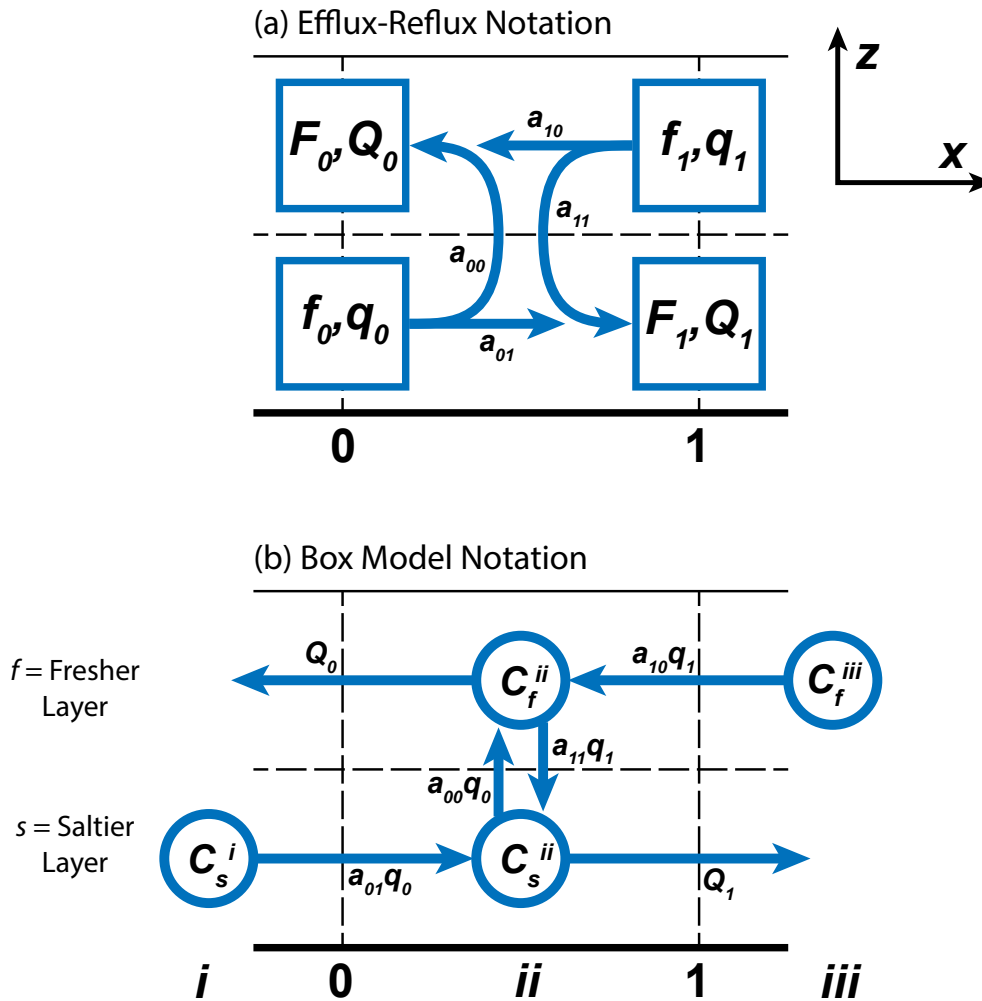
875

876

877   Figure 7. Sketch of notations used for (a) the efflux-reflux calculations, and (b) the box model.

878   Each panel represents three segments (*i-iii*) divided by sections 0 and 1. Each segment has two

879   layers in the vertical, a deep saltier one and a shallow fresher one. TEF volume and salt fluxes

880   are denoted by Q, q, and F, f in (a), and the efflux-reflux fractions are a_{00} and so on ($a_{from,to}$). In

881   the box model (b) C denotes the concentration of an arbitrary tracer, and the subscripts f and s

882   denote the "vertical" delineation.

883

884
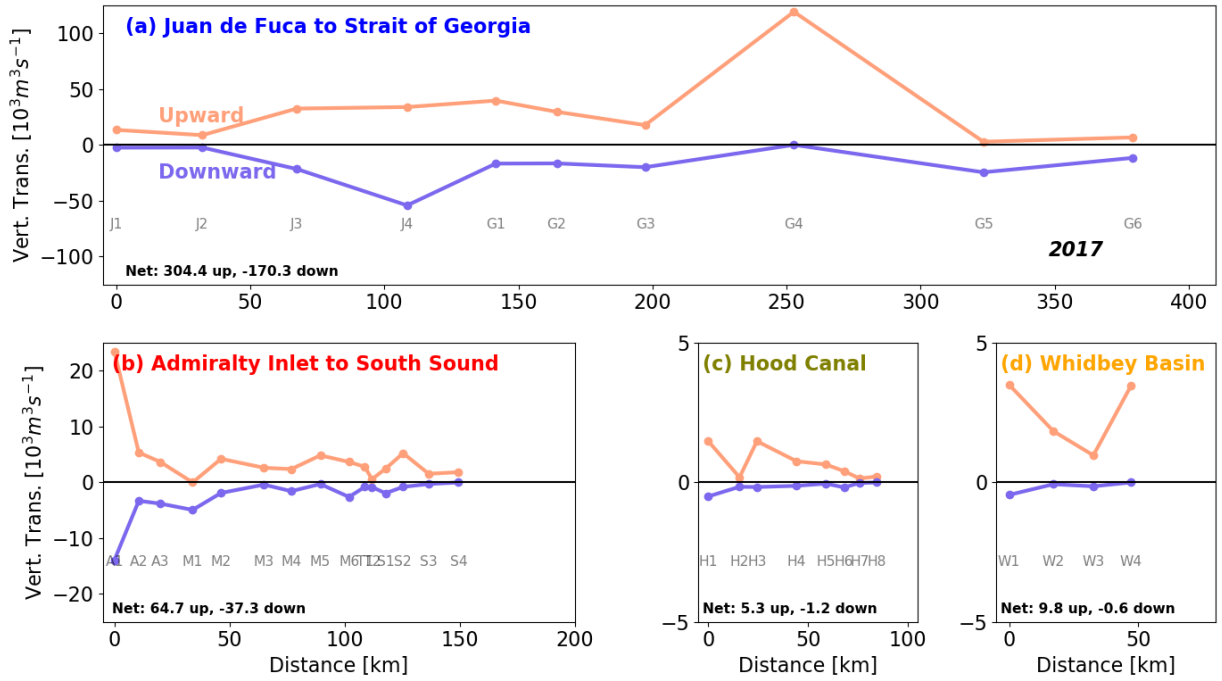
Figure 8. Vertical transports in segments for each channel from the efflux-reflux box model. Values shown are for the full year 2017. In each segment there may be both upward and downward transports, which is an alternate way of quantifying the effects of vertical advection and mixing. Note that the y-axis scales change for each panel. The sum of all up or down transports in each channel is shown in text at the lower left [10^3 m^{3}s^{-1}].
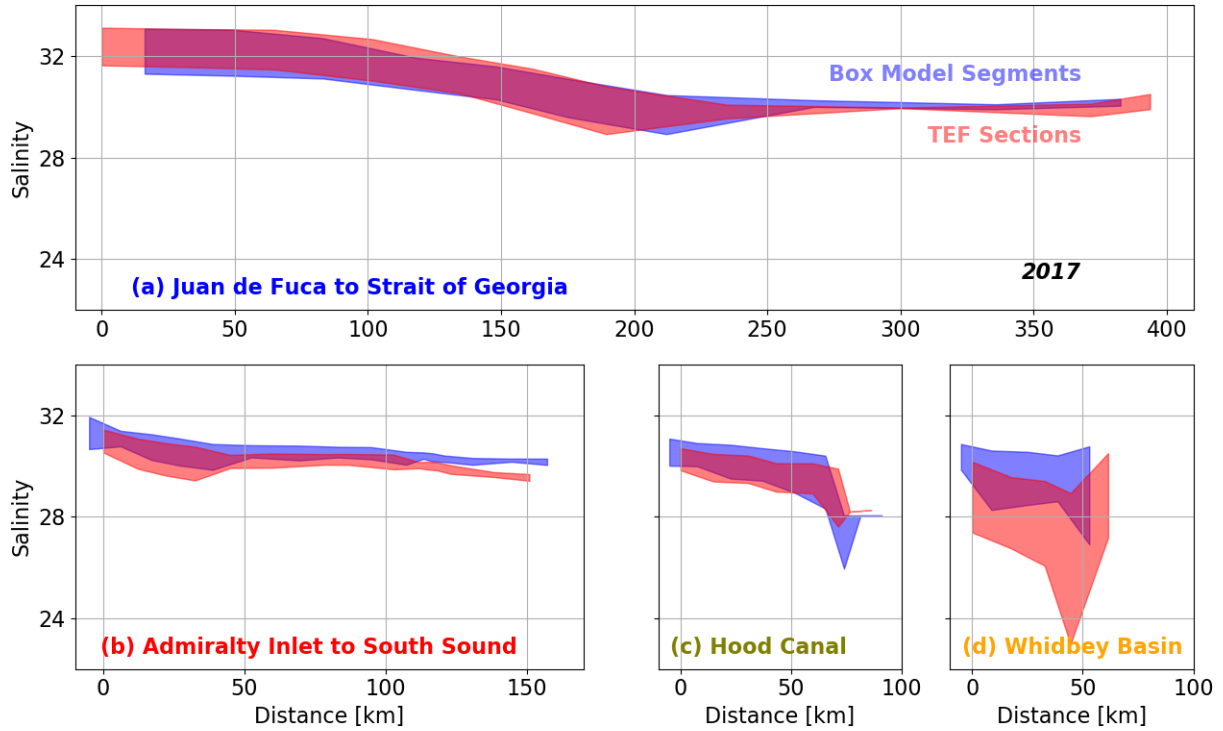
Figure 9. Test of the ability of the box model to reproduce the TEF salinities that were used to construct it. Each panel is for one of the four channels of the Salish Sea, and shows the range between upper- and lower-layer salinities as the vertical line thickness, vs. along channel distance. For the box model these salinities are in the segments, whereas for the TEF sections they are S_{out} and S_{in} on the sections.

904

905
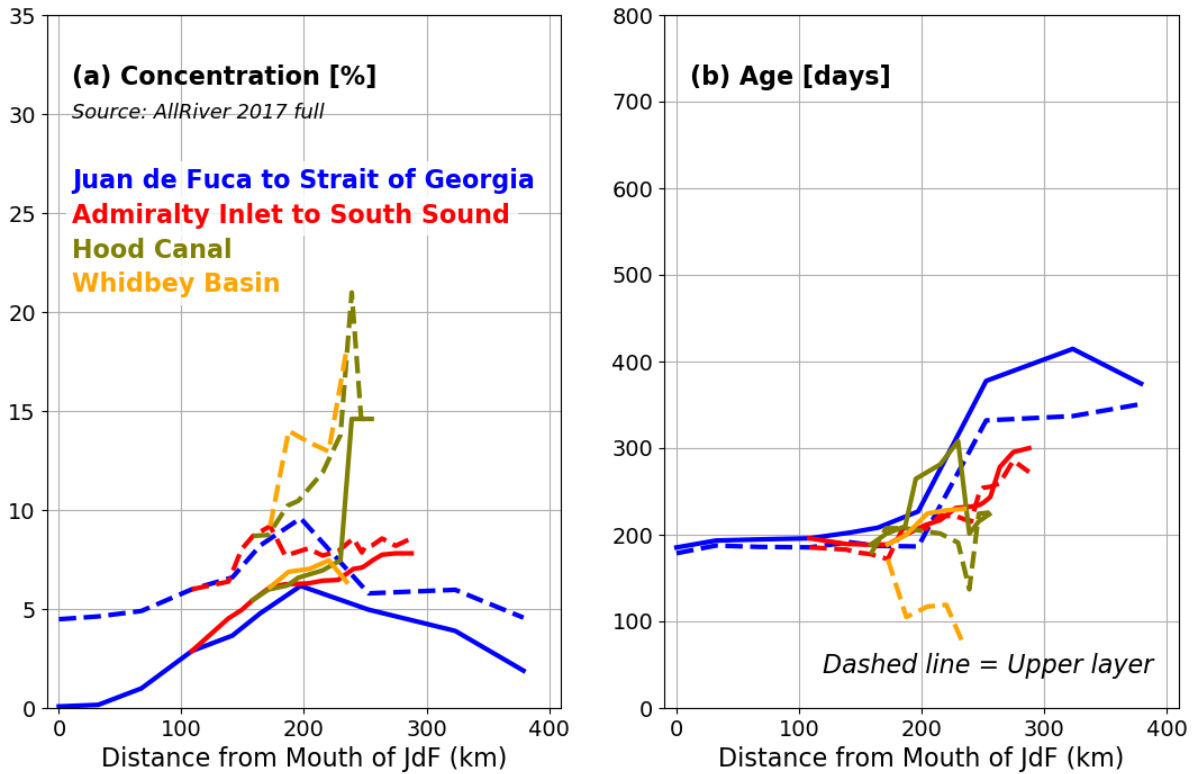
906

907

908

909 Figure 10. Result for the final state of a box model source experiment with a tracer of

910 concentration 1 coming out of all the rivers. The circulation, mixing, and river flows are

911 assumed to have the values of the mean of 2017 for the entire six-year integration. Final

912 concentration is shown in (a) and age in (b). The solid lines are the bottom sub-volumes of each

913 segment, and the dashed lines are for the surface sub-volumes.

914

915
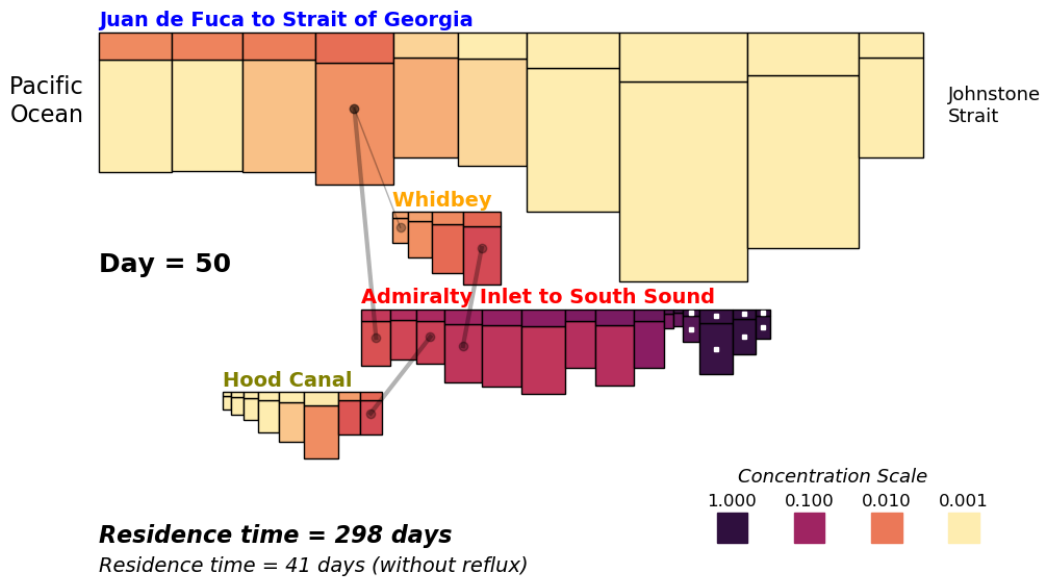
Figure 11. Snapshot of a time-dependent integration of a box model experiment in which there is a tracer initial condition, but no tracer coming in from the river or ocean sources. In this case the tracer was set to 1 in the volumes of South Sound (dark color with white squares) and allowed to advect and mix at rates from winter 2019. The snapshot is from 50 days into the integration, with color indicating $\log_{10}$ of the concentration. Each segment is shown as a rectangle (divided into upper and lower sub-volumes) and the rectangle size is proportional to segment volume. Connections between channels are shown as gray lines – the thin gray line connecting Whidbey Basin to the Strait of Juan de Fuca is Deception Pass.
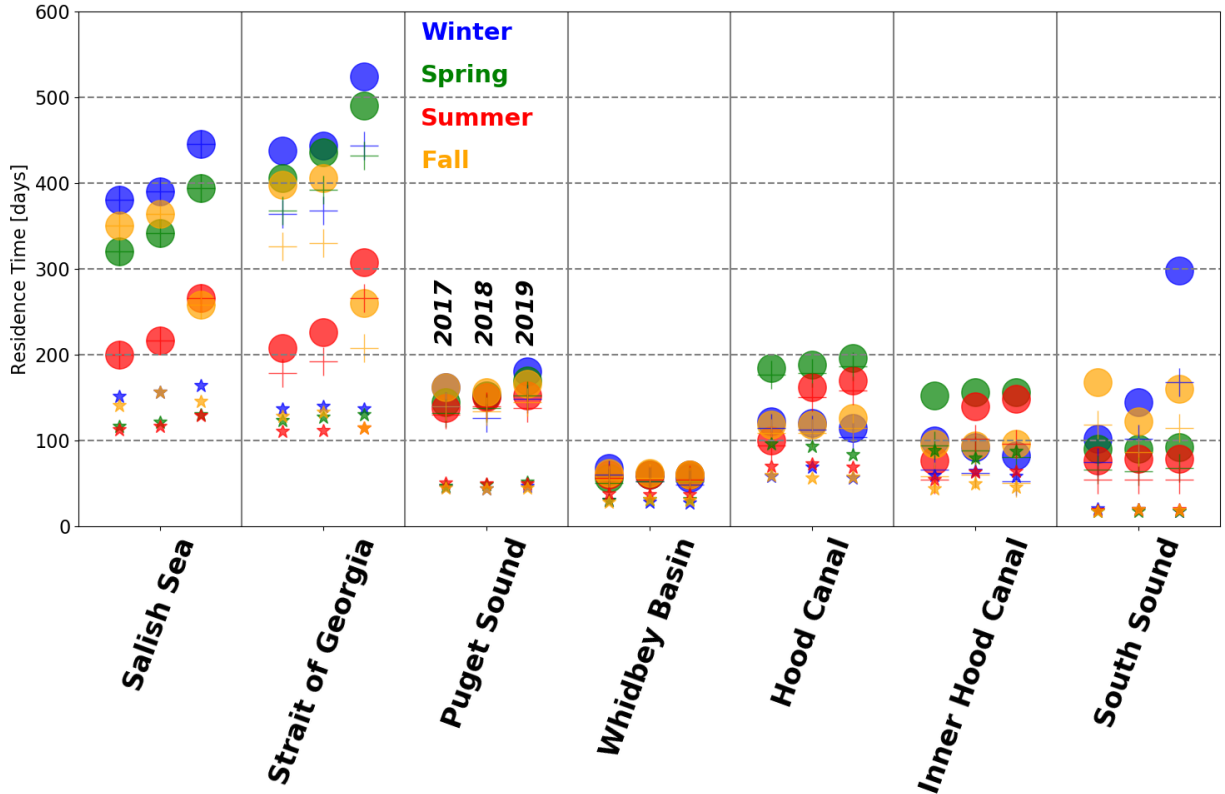
928

929

930   Figure 12. Residence times from box model initial condition experiments for various basins in

931   four seasons (colors). Each basin has values for three different years (separated horizontally as

932   indicated for Puget Sound). The large filled circles are T_{res}, the residence times calculated from

933   the box model as the *e*-folding time of a tracer initialized with concentration 1 in the segments of

934   that basin and 0 elsewhere. The smaller stars are T_{flush}. The crosses are T_{resNX}. The Hood Canal

935   Inner volume consists of just the deeper portions of segments H3-H8.

936

937

938

	T_{res}	T_{resNX}	T_{flush}	f_{reflux}	Sutherland et al. (2011)	Pawlowicz et al. (2007)
Salish Sea	327	327	136	0%		
Strait of Georgia	379	322	125	22%		112-319
Puget Sound	157	138	47	17%	57	
Whidbey Basin	60	53	31	24%	24	
Hood Canal	143	134	70	13%	81	
Hood Canal Inner	116	72	63	83%		
South Sound	125	85	18	37%	21	

939

940

941 Table 1. Residence and flushing times in days, averaged over all years and seasons in each basin

942 (Fig. 12) are given in the left three columns. Three different timescales are given, as defined in

943 the text, along with the fraction f_{reflux} by which T_{res} is changed when reflux is not included.

944 Comparisons to selected previous results are shown in the right two columns, as discussed in the

945 text.

946